NOTICE

The quality of this microform is heavily dependent upon the quality of the original thesis submitted for microfilming. Every effort has been made to ensure the highest quality of reproduction possible.

If pages are missing, contact the university which granted the degree.

Some pages may have indistinct print especially if the original pages were typed with a poor typewriter ribbon or if the university sent us an inferior photocopy.

Reproduction in full or in part of this microform is governed by the Canadian Copyright Act, R.S.C. 1970, c. C-30, and subsequent amendments.

AVIS

La qualité de cette microforme dépend grandement de la qualité de la thèse soumise au microfilmage. Nous avons tout fait pour assurer une qualité supérieure de reproduction.

S'il manque des pages, veuillez communiquer avec l'université qui a conféré le grade.

La qualité d'impression de certaines pages peut laisser à désirer, surtout si les pages originales ont été dactylographiées à l'aide d'un ruban usé ou si l'université nous a fait parvenir une photocopie de qualité inférieure.

La reproduction, même partielle, de cette microforme est soumise à la Loi canadienne sur le droit d'auteur, SRC 1970, c. C-30, et ses amendements subséquents.

THE UNIVERSITY OF ALBERTA

Migration of Dense Aqueous Phase Liquids in Homogeneous and Heterogeneous Porous Media

by

Robert Anthony Schincariol

A THESIS

SUBMITTED TO THE FACULTY OF GRADUATE STUDIES

AND RESEARCH IN PARTIAL FULFILLMENT OF THE

REQUIREMENTS FOR THE DEGREE OF Master of Science

DEPARTMENT OF GEOLOGY

EDMONTON, ALBERTA

SPRING, 1989

ISBN 0-315-52773-0

THE UNIVERSITY OF ALBERTA

RELEASE FORM

NAME OF AUTHOR: Robert Anthony Schincariol

TITLE OF THESIS: Migration of Dense Aqueous Phase Liquids in Homogeneous and Heterogeneous Porous Media

DEGREE: Master of Science

YEAR THIS DEGREE GRANTED: Spring, 1989

Robert Schincariol

18322 Old Young St.
Holland Landing
Ontario L0G 1H0

Date: Nov 25 1988

THE UNT ERSITY OF ALBERTA

FACULTY OF GRADUATE STUDIES AND RESEARCH

The undersigned certify that they have read, and recommend to the Faculty of Graduate Studies and Research for acceptance, a thesis entitled Migration of Dense Aqueous Phase Liquids in Homogeneous and Heterogeneous Porous Media submitted by Robert Anthony Schincariol in partial fulfilment of the requirements for the degree of Master of Science

Frank W. Schwartz
.....
Supervisor

.....

.....

.....

Date: Nov 25 1988

ABSTRACT

An experimental investigation into the migration of dense aqueous phase liquids (DAPLs) in homogeneous, layered and lenticular porous media has been conducted. In order to assess the effect of density on plume migration, a solution of 500 mg/L Rhodamine WT dye served as the carrier for various concentrations of solute (NaCl) introduced into a flow tank in varying concentrations from 1000 to 100,000 mg/L. An image analysis computer was used to obtain concentration distributions from the black and white photographs of the plumes. Density differences as low as 0.0008 g/cm^3 (1000 mg/L NaCl) between the DAPL and ambient groundwater in a homogeneous medium were found to cause convective dispersion and gravitational instability development at realistic groundwater velocities. As the density difference is increased to 0.0015 g/cm^3 (2000 mg/L NaCl), 0.0037 g/cm^3 (5000 mg/L NaCl) or higher, convective dispersion significantly alters the dispersion process, resulting in a large degree of vertical spreading of the plume so that the entire plume may enter a transient state. Heterogeneities are seen to greatly influence plume fall. In a layered medium, reductions in hydraulic conductivity on the order of half an order of magnitude

or less can retard gravitational free convection of the DAPL, and mass buildup along horizontal bedding interfaces can result in plume migration velocities up to 34% greater than ambient groundwater velocities for the solute concentrations and experimental conditions described herein. Small variations in hydraulic conductivity in the form of lenses act to retard plume fall, mask instability development and bifurcate the plume, resulting in a highly dispersed plume. An equation is presented that can provide a means to determine when density dependent effects need to be considered in a homogeneous isotropic medium.

ACKNOWLEDGEMENTS

I extend my appreciation to my supervisor, Dr. F.W. Schwartz, for his guidance, support, and constant quest to explore innovative and applied areas of research. The comments and suggestions made by the members of my examining committee, Dr. J. Tóth, Dr. T.F. Moslow and Dr. D.C. Sego are gratefully acknowledged. I must also extend my appreciation to Dr. F. Schwille, Federal Institute for Hydrology, Koblenz (F.R.G.), Dr. L. Hull, Idaho National Engineering Laboratory and R.C. Starr, University of Waterloo, for their expert advice on experimental design and operation of flow tanks. The many stimulating discussions with my colleagues Joao Kupper, Allan Crowe, Gordon McClymont, Ben Rostron and Alan Fryar are greatly appreciated. I would also like to thank Morris Maccagno for running the permeameter tests.

Funding for the project was provided by Imperial Oil University Research Grants, 1988/1987, and NSERC operating grants to Dr. F.W. Schwartz.

TABLE OF CONTENTS

Chapter Page

1. INTRODUCTION 1

2. EXPERIMENTAL METHOD 4
   2.1 Flow Tank Design 5
   2.2 Porous Medium Type and Emplacement Procedure .9
   2.3 Wall Effects 11
   2.4 Tracing Plume Migration 13
      2.4.1 Image Analysis 14

3. EXPERIMENTAL RESULTS 19
   3.1 General Description of the Three Media Trials 19
   3.2 Homogeneous Medium 26
   3.3 Layered Medium 37
   3.4 Lenticular Medium 48

4. DISCUSSION 56

5. CONCLUSIONS 71

REFERENCES 74

APPENDIX 77

LIST OF TABLES

Table		Page
1	Solute Concentration in Relation to Binary Images	18
2.	Porous Media Data	20
3.	Experimental Data for Homogeneous Medium Runs	28
4.	Average Linear Velocities for Each Layer	41
5.	Horizontal versus Inclined Strata Plume Velocities	47
6.	Experimental Data for Lenticular Media Runs	49
7.	Calculation of v and v_R for Various Experiments in the Homogeneous Medium	58
8.	Hydrodynamic Dispersion Coefficients	62

LIST OF FIGURES

Figure		Page
1	Diagrammatic Plan of Flow Tank	6
2	Porous Metal Plate Inset	8
3	Binary Images of 250-125-50-25 mg/L Rhodamine WT Distribution	16
4	Gradation Curves	22
5	Hydraulic Conductivity Distribution for the Layered Medium Experiments	24
6	Hydraulic Conductivity Distribution for the Lenticular Medium Experiments	25
7	Binary Images for a 5000 mg/L NaCl Source in Homogeneous Medium at Various Times	29
8	Binary Images for Various Source Concentrations in Homogeneous Medium at 54 Hours	31
9	Binary Image for a 100,000 mg/L NaCl Source in Homogeneous Medium at 18 Hours	34
10	Instability Development Over Time for a 2000 mg/L Nacl Source in Homogeneous Medium	35
11	Plume Outlines for 500 mg/L Rh(WT) and 5000 mg/L Nacl (High Velocity) Source in Homogeneous Medium	36
12	Plume Outline of 5000 mg/L NaCl Source Run in Homogeneous Medium 12 Hours After Velocity Decrease from 5.67×10^{-3} to 3.00×10^{-4} cm/s	38
13	Plume Outlines of Two 2000 mg/L NaCl Plumes at 54 Hours	39
14	Binary Images for a 5000 mg/L NaCl Source in layered Medium at Various Times	43
15	Binary Images for a 10,000 mg/L NaCl Source in Layered Medium at Various Times	44
16	Plume Outlines for Various Source Concentrations in Layered Medium at t=12 Hours	46

Figure Page

17 Binary Images for Various Source Concentrations in Lenticular Medium at t=72 Hours 50

18 Binary Images for a 5000 mg/L NaCl Source in Lenticular Medium at Various Times 52

19 Binary Images for a 10,000 mg/L NaCl Source in Lenticular Medium at Various Times 54

20 Forces That Act on a Given Fluid Element 57

1. INTRODUCTION

In many problems involving contaminants dissolved in water, the plume will have a chemical composition and density that is different from the native groundwater. The differences in density appear to have an important influence on mass transport. For example, there is a general awareness that a dense plume will sink. However, a clear conceptual understanding of the variable density transport problem is lacking.

Part of the problem is the relatively small number of studies that have looked at how fluids with different densities behave, specifically the trajectory and mechanism of plume fall within an ambient native groundwater flow field. Wooding (1959, 1962, 1963, 1969) and Bachmat and Elrick (1970) studied theoretically and experimentally the hydrodynamics and vertical convection between two miscible fluids of varying density in a porous medium without an ambient groundwater flow field. List (1965) and Paschke and Hoopes (1984) also studied theoretically and experimentally the motion and mixing of dense aqueous phase liquids (DAPLs) in a manner analogous to that used in hydraulics with jets and plumes discharging into an ambient crossflow. These studies

dealt with homogeneous media but with large ambient groundwater flow velocities (2700 to 5010 cm/day). Recently Herbert, Jackson and Lever (1987) attempted to model numerically the groundwater flow over a hypothetical salt dome, incorporating the effects of significant density variations due to high salt concentrations. Those workers encountered difficulties with the non-linearities arising from the density variation and the velocity-dependent dispersion tensor. Other "variable-density groundwater flow work" such as Davies (1987) has dealt with areal, not vertical, variations in fluid density and how the density-related gravity effects can change flow directions and velocities with planar dipping aquifers. There has been considerable field and theoretical work in looking at the dynamics of mixing between freshwater and seawater. However, the dynamics of this mixing process is much different from the case of interest here, and it will not be considered further.

The vertical migration of DAPLs, to my knowledge, has not been studied at realistic groundwater velocities or in heterogeneous systems. The objective of this study has been to conduct experiments enabling me to explore flow phenomena that have been largely unexplored previously in either experimental or theoretical work.

The approach adopted here is an experimental one that describes the migration of DAPLs under typical groundwater conditions (velocities, hydraulic conductivities and boundary conditions). The specific objectives of the work are to evaluate the influence of the density of a plume on its migration path and the conditions under which density differences become significant. In order to assess the effect of density on plume migration, a solute (NaCl) has been introduced into a flow tank in varying concentrations from 1000 mg/L to 25,000 mg/L NaCl. First, a homogeneous medium has been used, then the effects of heterogeneities have been studied with two cases, a layered medium and a lenticular medium. This allows me to gain an understanding of how DAPLs will behave when they encounter heterogeneities under typical field conditions.

2. EXPERIMENTAL METHOD

An integral part of this study has been to construct a physical model or flow tank that can accurately reproduce groundwater conditions. For the purposes of this study the model had to produce a uniform, groundwater flow field at typical groundwater flow velocities for a variety of different spatial distributions of hydraulic conductivity. One of the limitations of earlier studies (List, 1965; Paschke and Hoopes, 1984) that needed to be avoided was unrealistically high groundwater flow velocities. The possibility exists that some density effects could be masked at these high flow velocities.

Another important requirement in the design was a capability for fully documenting patterns of tracer spread with minimal disturbance of the flow field. In this study, a visual approach has been chosen as the monitoring scheme. The tank was constructed with Plexiglas walls to permit the plume spreading to be photographed. Other monitoring techniques (e.g., electrodes or sample ports) would require a prohibitively large number of sample points to describe the plume conditions accurately, and could lead to apparatus-induced heterogeneities. It is the acquisition of in-

situ measurements of solute concentrations, without disturbing the flow field, that is generally the stumbling block in obtaining data in laboratory studies (Cahill, 1973).

2.1 Flow Tank Design

The laboratory model has internal dimensions of 116.8 cm in length, 71.0 cm in width, and 5 cm in depth. It was constructed of 1.8 cm Plexiglas according to the diagrammatic plan shown in Figure 1. The length and width dimensions are such that the travel path of the tracer is sufficiently long to show the effects of plume density. The thickness has been selected to provide a sufficiently large cross-sectional area so that realistic flow rates could be produced using a volumetric displacement pump.

The use of Plexiglas inherently requires lateral support to prevent the bulging of the walls. To this end, nine strategically placed 5 mm diameter tie rods have been used to keep the walls plumb. However, only three are placed within the porous media to avoid disrupting the flow field to any great extent.

Influent and effluent reservoirs are placed at each end of the tank. They buffer the effect of the inflow/outflow lines by redistributing the flow across the porous medium. Porous metal plates keep the sand out

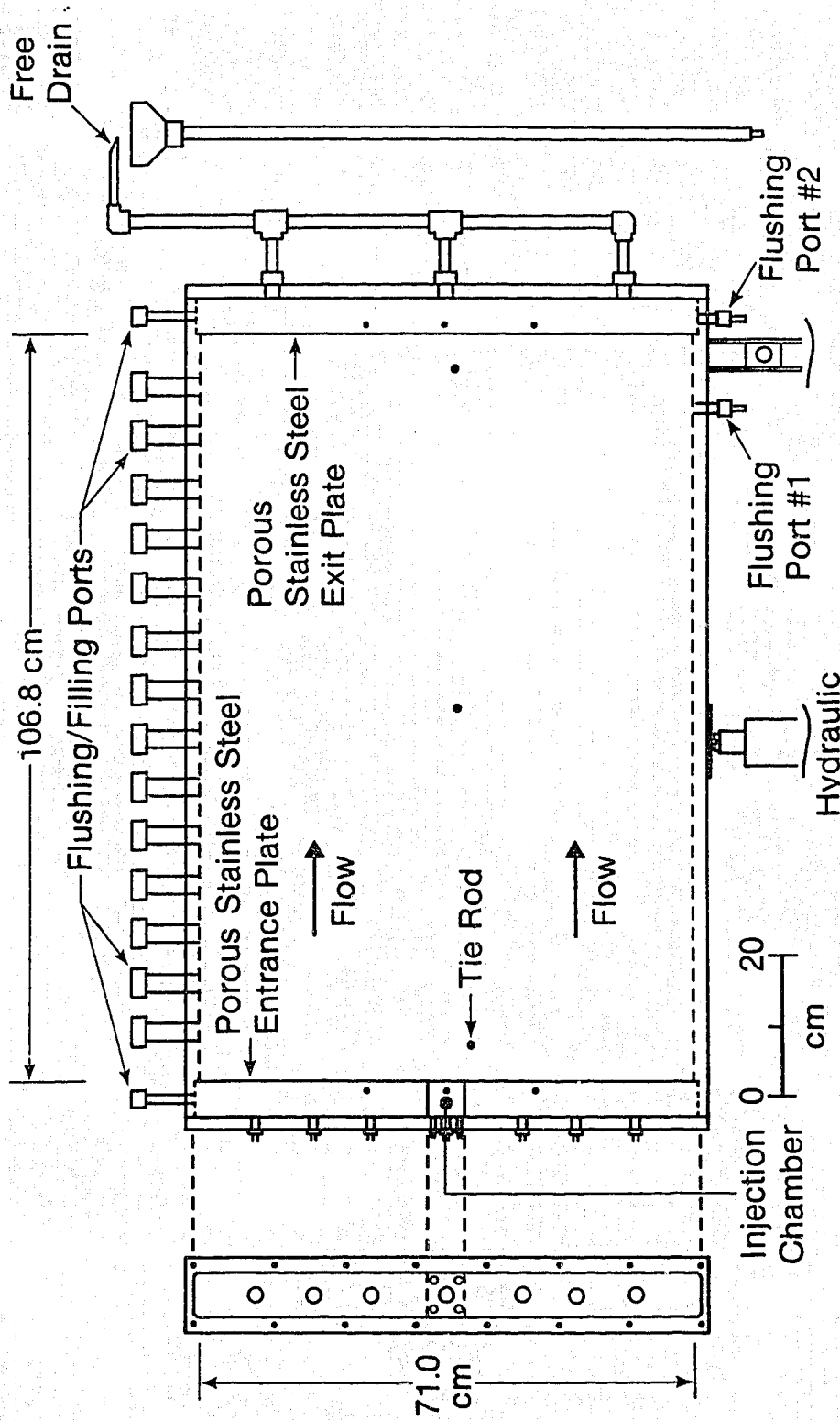

Figure 1. Diagrammatic Plan of Flow Tank

of the reservoirs. The porous metal plates are manufactured from 316L stainless steel (Mott Metallurgical Corporation, Farmington, Conn.), are 1.6 mm thick and have an interconnected porosity of 50 percent with a 20 micron pore diameter.

The influent and effluent reservoirs have been cut a few millimeters longer and deeper than the dimensions of the porous media chamber so that the porous metal plates could be recessed and sealed along the plexiglass wall. This feature helps to keep the flow field uniform with no wall/plate contact effects (Figure 2). To further decrease entrance effects, seven influent lines and three effluent lines have been used. Both ends of the tank are removable and are sealed in place utilizing O-ring seals.

The injection chamber is formed by sealing in place with silicone two 5cm x 5cm x 0.5cm thick plexiglas squares. The dimensions of the injection chamber can thus be varied. In order to provide an "instantaneous" injection front, with little disruption of the flow field, four injection/withdrawal ports have been installed. The use of a syringe mechanism, one syringe withdrawing contaminant plus ambient water and one injecting the contaminant at exactly the same rate, enables the establishment of an "instantaneous contaminant front" across the full dimensions of the

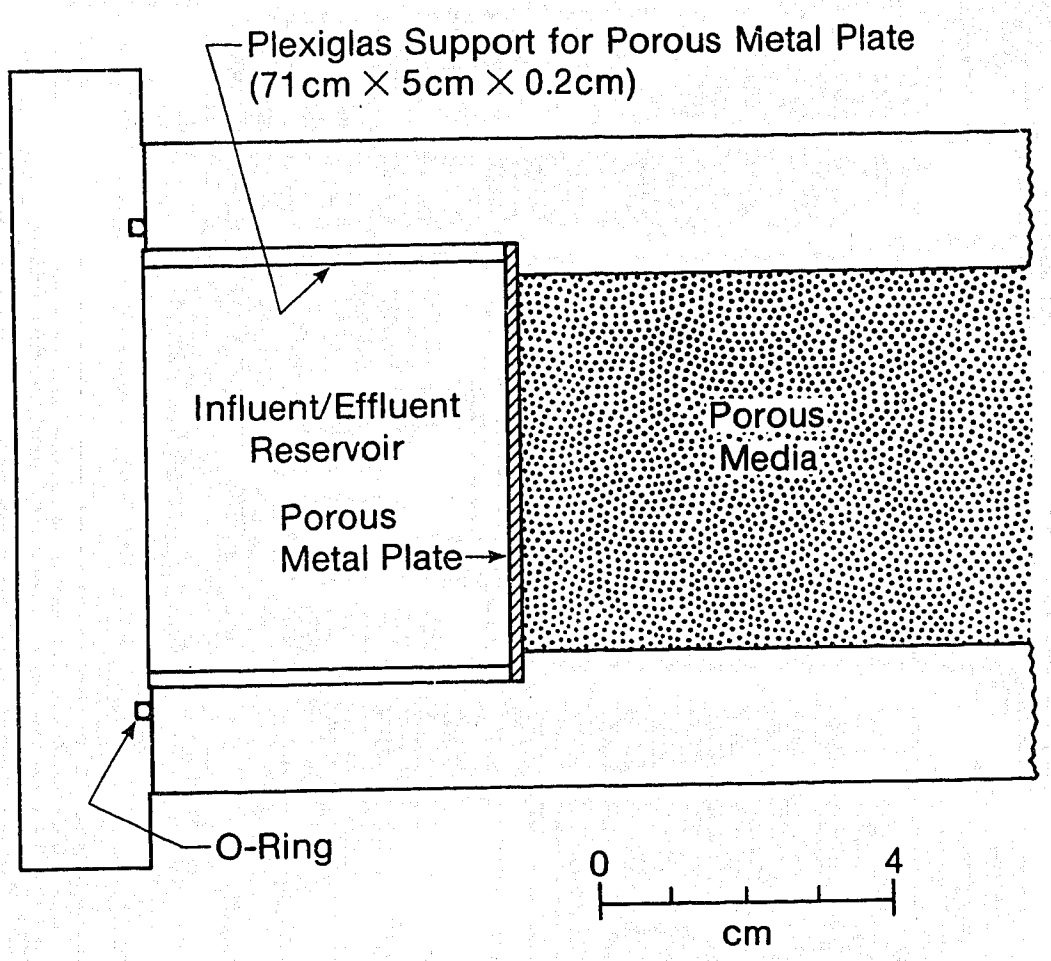

Figure 2. Porous Metal Plate Inset

injection chamber without disturbing the ambient flow field.

Peripheral equipment includes an autoanalysis multichannel peristaltic metering pump coupled with in-line flowmeters at the influent end of the tank. The pump (Ismatec. schlauchpumpe mv-ge, Cole-Parmer Instrument Company, Chicago, Illinois), capable of consistently delivering as little as 0.02 ml/min., is the key to operating the flowtank at low flow velocities.

2.2 Porous Media Type and Emplacement Procedure

The porous media consist of various sizes of industrial glass beads. The glass beads are obtainable in various size categories, are spherical, smooth, and do not scratch the plexiglas walls easily. Their light colour also enables the dyed plumes to be easily visible.

Filling the tank with glass beads to obtain a uniform packing with little entrapped air posed some problems. The typical technique, which involves pouring and emplacing the beads or sand under water and then vibrating or compacting the sand consistently (Todd (1980), Bear (1972), and Cahill (1973)), could not be used effectively with this tank. First, the glass beads are not perfectly uniform and so variation in fall velocity causes some layering. This structure can be tolerated in the studies of heterogeneous media but not

for the homogeneous medium. Second, the lack of steel reinforcing structural supports on the tank does not allow the use of heavy vibration. Therefore, a new technique has been developed that has proven to be effective.

For the homogeneous medium, the dry tank is tilted 90 degrees on its end and the glass beads are rapidly poured inside. About 23 kilograms of beads are poured at a time in three increments. When the beads are poured rapidly, variation in fall velocity only affects the end of each pour. Layering is minimized, and any that does develop is perpendicular to the flow direction. Once the tank is filled the porous metal plates are sealed in place, the end is closed, and the tank is rotated back into its normal position. The tank is then flushed with CO_2 through the lower flushing port #1 (Figure 1) at a rate of 5 L/min. for about 1.5 hours (approximately 25 pore volumes). Flushing with CO_2 serves two purposes. First, as in Sudicky et al. (1985), the CO_2 is used to displace air in the porous medium. Then, during saturation with water, the CO_2 occupies voids that are otherwise occupied by air and, because the CO_2 is approximately 40 times more soluble in water than air (CRC, 1981), the remaining gas is less likely to be trapped at residual saturation. Saturation and flushing

with CO_2 also provide an effective way of compacting the porous medium. In the first few minutes of flushing, in the homogeneous medium case, the porous medium compacts one to two centimeters. After saturation with CO_2, the flushing ports are closed, the upper flushing/filling ports are used to add sufficient glass beads to top off the tank, and deionized, deaired water is pumped in through the bottom of flushing port #1. The upward movement of water displaces most of the CO_2 from the pores and no entrapped CO_2 is observed along the walls. Deionized, deaired water is next run at high velocities of 9.3×10^{-3} to 1.2×10^{-2} cm/s to compact further the medium and dissolve and/or displace any entrapped CO_2. The upper flushing/filling ports are then used again to top off the porous medium, and plastic rods are hammered into place to provide a tight pack at the top of the tank and prevent any short-circuiting of the flow.

In the heterogeneous cases a similar procedure to that outlined above has been used, except the filling/flushing ports are used to fill the tank from the start, and longer CO_2 flushing times are employed.

2.3 Wall Effects

The significance of wall effects needs to be addressed, because all measurements will essentially be viewed against the walls of the tank. It is clear that

the wall will affect the flow in its immediate vicinity and a given number of grain diameters beyond this. Dudgeon (1967) did a thorough experimental investigation of wall effects in relation to permeameter studies. He studied the porosity change and the resulting velocity distortion at the walls in both rectangular boxes and cylindrical columns. For non-cohesive granular and spherical media, "the gross increase in local porosity near the wall should be restricted to a zone whose average width is of the order of half a median particle diameter: (Dudgeon, 1967). The mean value of the ratio of the porosity at the wall zone to the over-all porosity was found to be approximately 1.3:1.

Schiegg and McBride (1987) also investigated the porosity of packed spheres along a smooth wall. They found the porosity is approximately 25 percent greater along the wall over four to five grain diameters, although the major influence can be seen to occur over the first grain diameter. In a preliminary investigation of my flow tank, wall effects seem to be of little importance. Dye fronts are uniform in colour, with no light areas showing much difference in velocity distribution (dye only travelling within the first few gain diameters would appear lighter in colour); in

addition, the breakthrough patterns along the exit porous metal plate were uniform.

2.4 Tracing Plume Migration

The dye used in tracing plume migration should be nonsorbing, nondegrading, relatively inert, and not influenced by NaCl, the selected solute. Rhodamine WT liquid (Crompton and Knowles Corp., Charlotte, NC) was found to have these attributes. Because Rhodamine WT [Rh(WT)] is anionic, it is not attracted by the negative charges present on most solid surfaces. In their evaluation of some fluorescent dyes for water tracing, Smart and Laidlaw (1977) found no significant adsorption of Rhodamine WT, on soft or hard glass, for periods of up to 10 weeks. My studies also have shown very minimal adsorption onto the glass beads and no adsorption onto the Plexiglas. Rhodamine WT also has a very low photochemical decay rate under both natural and artificial light (Smart and Laidlaw, 1979). Other tests on Rhodamine WT solutions in distilled water indicated that dye concentration was not affected by exposure to laboratory fluorescent lights, and that no significant decay of Rhodamine WT occurred due to salinity (NaCl) effects (Stanbro and Pyrch, 1979).

In my studies, a solution of 500 mg/L Rhodamine WT liquid in water has served as the carrier for various

concentrations of solute. This concentration is sufficiently dark to clearly show the transport paths yet has a density close enough to the ambient fluid, distilled water, so that no density effects are apparent. The Rhodamine dye is actually visible under normal room light conditions in the porous media to concentrations of at least 5 to 10 mg/L. Although Rhodamine WT is detectable by fluorometry to concentrations as low as 0.013 micrograms per litre, the dye has not been traced by fluorescence in this study.

2.4.1 Image Analysis

A Tracor Northern 5500 Image Analysis computer was used to obtain concentration distributions from the black and white photographs of the plumes. A gray scale was placed on the tank so that small differences in lighting conditions and processing would not affect the uniformity of gray levels from photograph to photograph.

The photographic method of measuring concentration distributions can be very effective providing extreme care is taken to ensure even lighting across the tank. My experiments did suffer from inability to control room lighting effectively. Variations across the tank due to lighting conditions at their extreme equaled approximately the gray level for 50 mg/L Rhodamine WT, or, since it is the dye, not the solute, which we are

visually detecting, about the last 10% of a given NaCl concentration tagged with 500 mg/L Rhodamine WT. In other words, I was not able to detect over background error concentration levels less than 10% of source concentration. Background subtractions were attempted, and did succeed in evening out the lighting, but also evened out the gray scale so that photograph to photograph uniformity was lost. Even if lighting conditions were improved, the low concentration zones that were visible on colour photographs were equal in gray tone to the slightly greenish tone of the glass beads.

In order to determine what gray level corresponds to what concentration of solute, I introduced known concentrations of Rhodamine WT into the tank and processed photographs from the test on the image analysis computer. I was only able, given the lighting and other problems, to delineate two gray levels or groups of levels within the tank which would give me reproducible and reliable results. Figure 3 shows the image printouts for two gray levels of a 250-125-50-25 mg/L Rhodamine WT distribution. One level, which I will refer to as the high concentration binary image (HCBI), represents a concentration of approximately 250-500 mg/L Rhodamine WT. This gray level appears as the solid black area on Figure

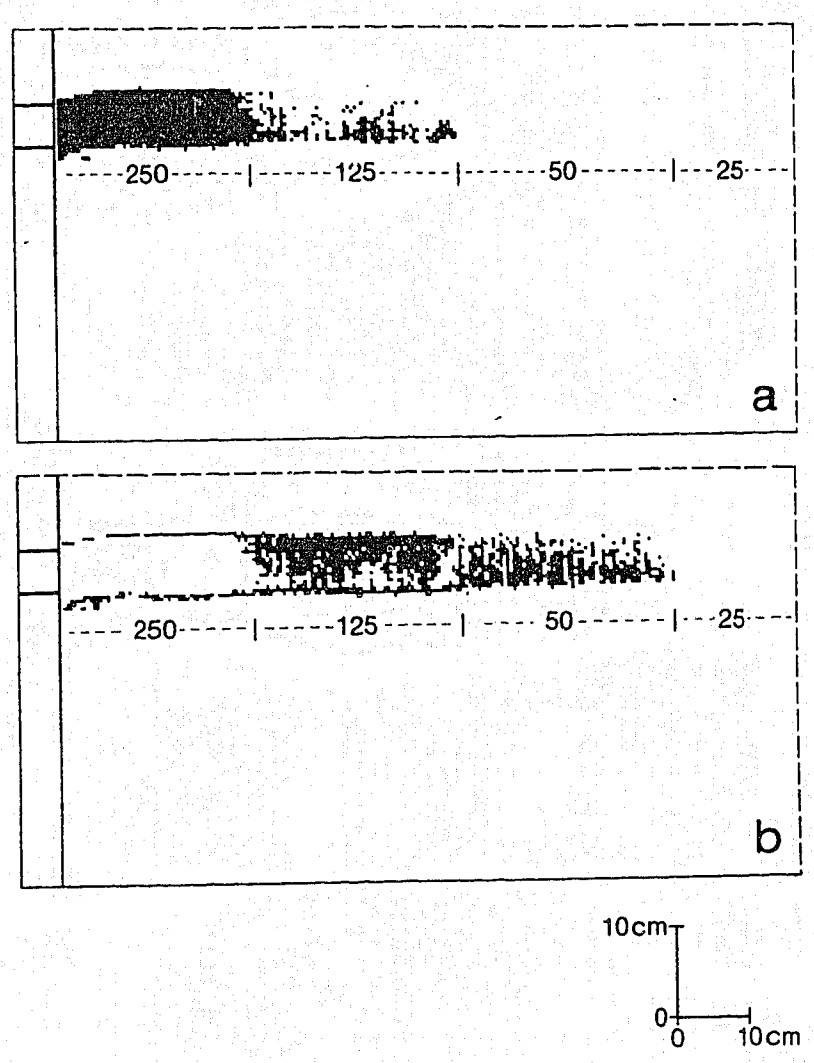

Figure 3. Binary Images of 250-125-50-25 mg/L Rhodamine WT Distribution. (a) HCBI; (b) LCBI

3a. The other level, which I will refer to as the low concentration binary image (LCBI), represents a concentration of approximately 50-125 mg/L Rhodamine WT (Figure 3b).

Overall, in the data to be presented in the following sections, the two gray level binary images will be combined such that the HCBI will appear as a stippled area and the LCBI will appear as the solid black area composed of pixels. The high concentration zone, useful in showing the bulk plume shape, corresponds to a 50-100% concentration level and the low concentration zone, showing the zone of dispersion, corresponds to a 10-25% concentration level (Table 1). The 25-50% concentration level can fall into either group as the gray tones in this range were inseparable.

Table 1. Solute Concentration in Relation to Binary Images

Solute Concentration (mg/L)	HCBI Approximates a Zone of (mg/L)	LCBI Approximates a Zone of (mg/L)
500 Rh (WT)	250 - 500	50 - 125
100000 NaCl	50000 - 100000	10000 - 25000
25000 NaCl	12500 - 25000	2500 - 6250
10000 NaCl	5000 - 10000	1000 - 2500
5000 NaCl	2500 - 5000	500 - 1250
2000 NaCl	1000 - 2000	200 - 500
1000 NaCl	500 - 1000	100 - 250

3. EXPERIMENTAL RESULTS

The experiments involved three different types of porous media: a homogeneous medium, a layered medium, and a lenticular medium. For each of the three media between 5 and 11 experimental trials were run using DAPLs with concentrations ranging from 1000 mg/L to 100,000 mg/L NaCl. The higher concentrations, 10,000 to 100,000 mg/L NaCl, correspond to typical leachate or source densities and the lower concentrations to more dilute plumes.

It should be noted that when the photographs are image processed the image is slightly compressed in the horizontal dimension and slightly expanded in the vertical dimension. Therefore, a horizontal and vertical scale is shown on each figure.

The following sections detail the media characteristics and experimental results.

3.1 General Description of the Three Media Trials

Constant head permeameter tests have been run on all size categories of glass beads used following standard procedures as outlined in Bowles (1978) and Das (1982). The manufacturer's (Canasphere Industries Ltd., Calgary, Alberta) size designation, mean grain size, and hydraulic conductivity values can be seen in Table 2. The

Table 2. Porous Media Data

Manufacturers Bead Size#	Median Grain size d_{50} (mm)	Hydraulic Conductivity (cm/s)		Typical Stratum Material
		Kozeny-Carman (n=0.38)	Permeameter Results	
3	0.650	2.9×10^{-1}	3.0×10^{-1}	Clean Sand to Gravel
5	0.310	6.6×10^{-2}	5.6×10^{-2}	Clean Sand
7	0.210	3.0×10^{-2}	2.2×10^{-2}	Clean Sand
10	0.150	1.6×10^{-2}	1.2×10^{-2}	Clean Sand
13	0.085	5.0×10^{-3}	1.9×10^{-3}	Silty Sand

hydraulic conductivity values in Table 2 represent a mean of 6 permeameter runs per sample, each run at varying head differences and standardized to 20 degrees Celsius. The hydraulic conductivity can also be estimated using the Kozeny-Carman equation (Bear, 1972), which takes the form,

$$K = \frac{(\rho g)}{\mu} \left[\frac{n^3}{(1-n)^2} \right] \frac{dm^2}{180} \qquad (2.1)$$

where K = hydraulic conductivity
ρ = fluid density
g = 980 cm/s
μ = fluid viscosity
n = porosity
dm= some mean particle size

Working with spherical glass beads the mean particle size, dm, can be taken as the sphere diameter (Bear, 1972). Because the glass beads are fairly uniform (see gradation curves, Figure 4), the d_{50}, or median grain size, can be taken as the dm. As expected, the Kozeny-Carman equation closely approximates the permeameter results (Table 2). It should also be noted that, due to the sphericity and uniform grain size of the glass beads, a smaller than normal grain size must be used to obtain a given hydraulic conductivity.

For the homogeneous medium experiments the tank was filled with size #5 glass beads. For the layered medium

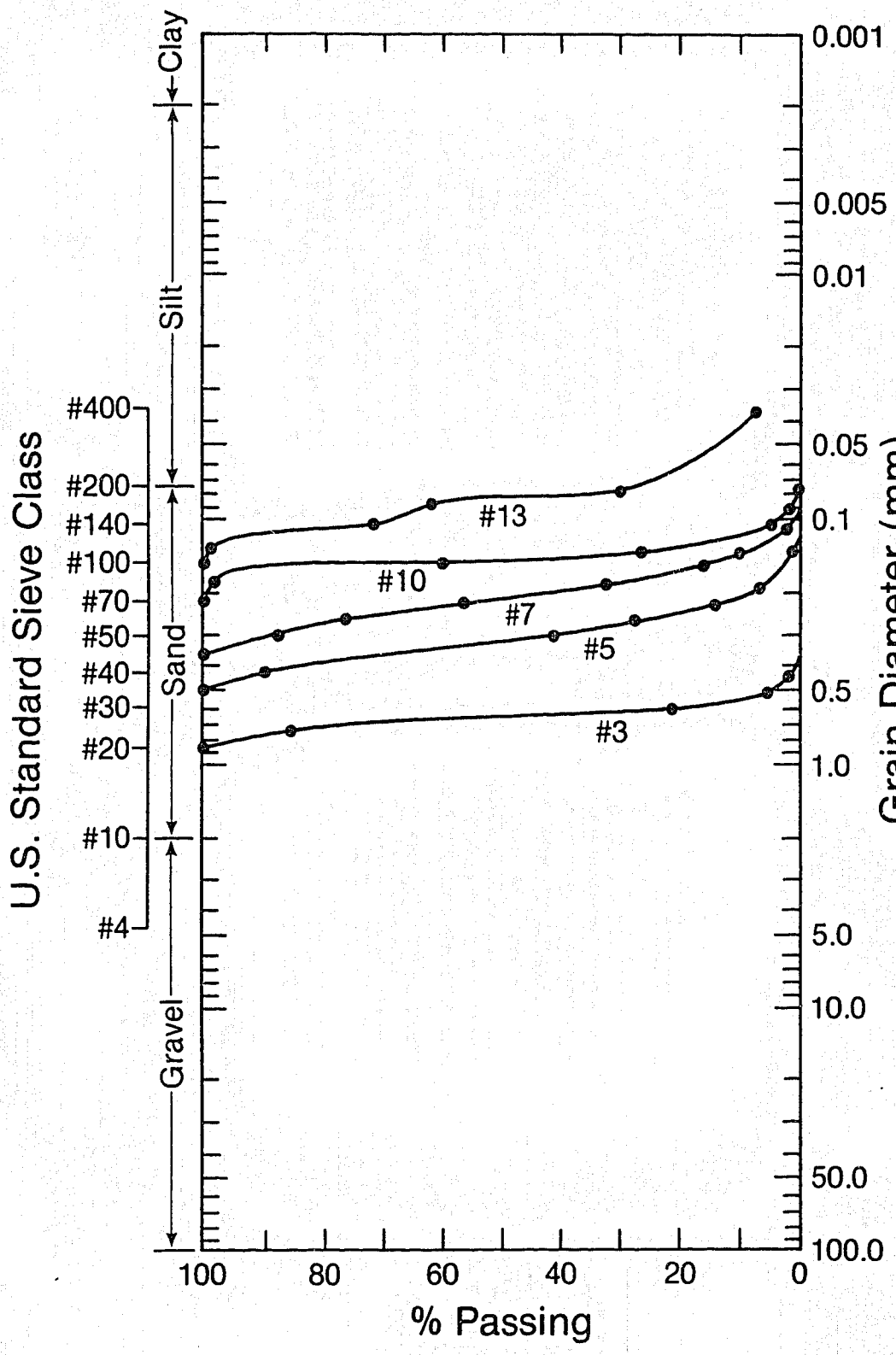

Figure 4. Gradation Curves

experiments the pattern of layering can be seen in Figure 5. The layers above and below the centre layer (size #3 glass beads) have progressively lower hydraulic conductivities. The complex distribution of hydraulic conductivity for the lenticular medium can be seen in Figure 6. Zones 1 and 3 consist solely of low hydraulic conductivity lenses while zone 2 consists of low and high conductivity lenses all contained within size #5 glass beads.

In all experimental runs the tracers were introduced through the 5cm x 5cm x 5cm injection chamber while deaired/deionized water was injected at the same specific discharge rate through the upper and lower influent reservoirs. The dimensions and position of the injection chamber remained the same for all runs (Figure 1). Prior to each experimental run the flow field was allowed to come to steady state, at the required velocity, overnight. After a run the tank was flushed with deaired/deionized water until all traces of the dye were gone. To make sure no NaCl remained in the water or was sorbed onto the media after the dye was visibly flushed out, preliminary experiments were run testing the effluent fluid for sodium by flame photometer. The exit water just after a 2000 mg/L NaCl plume was visibly flushed out had a Na^+ concentration of 4.7 mg/L (ambient

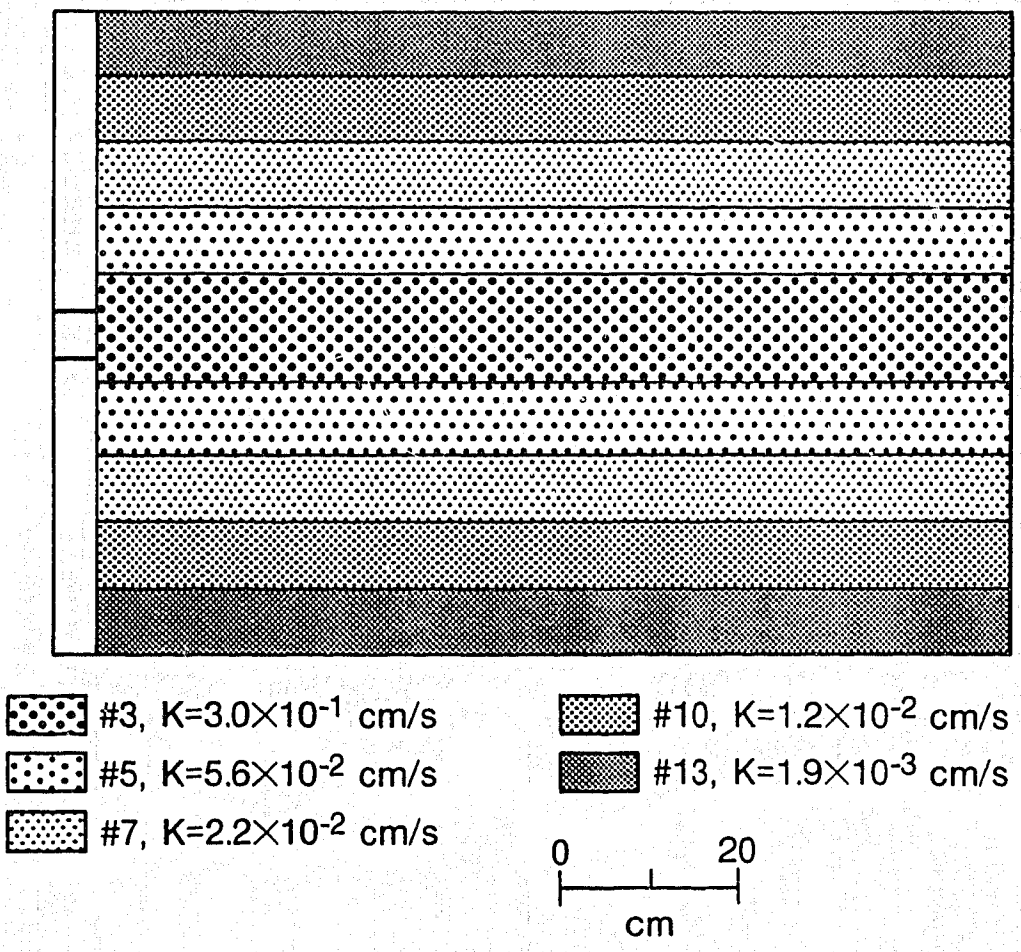

Figure 5. Hydraulic Conductivity Distribution for the Layered Medium Experiments

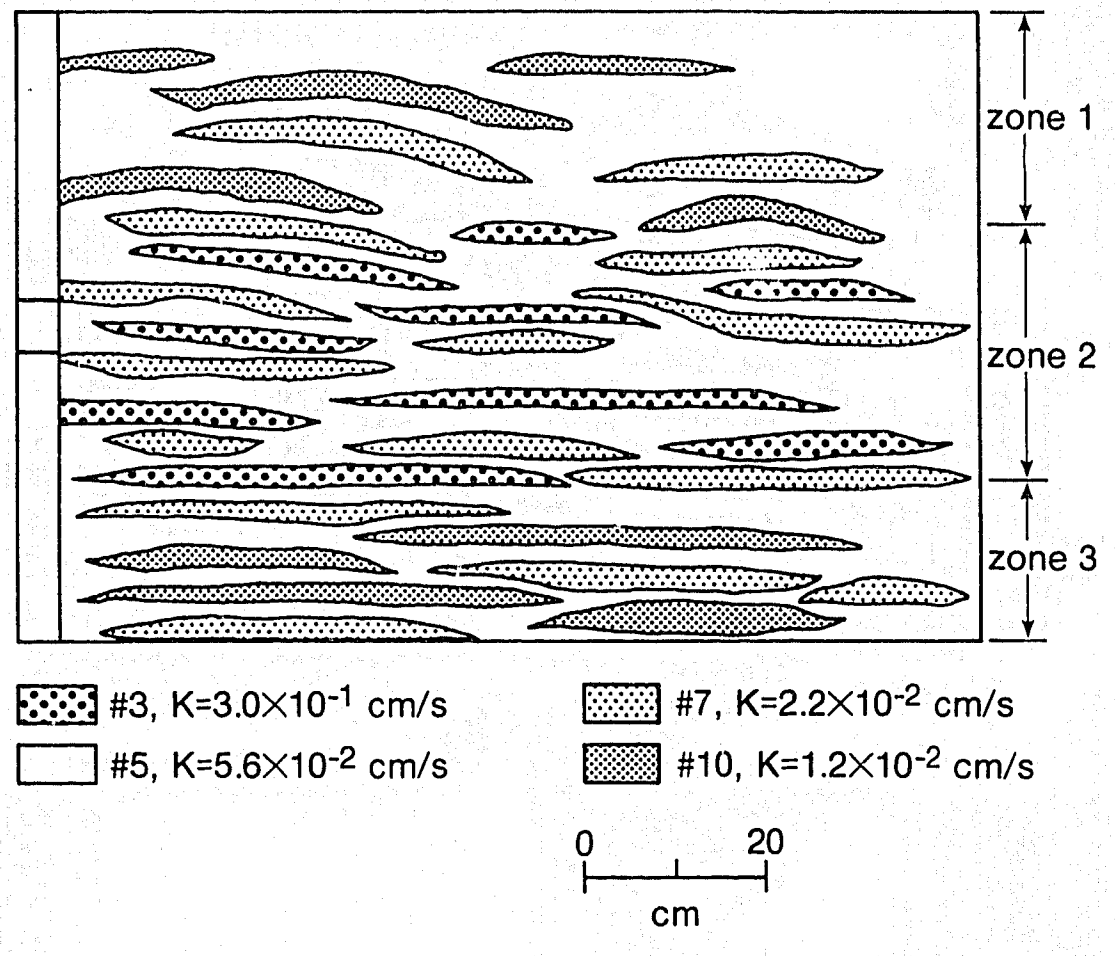

Figure 6. Hydraulic Conductivity Distribution for the Lenticular Medium Experiments

water entering tank had a Na^+ concentration of 3.6 mg/L). These results show that as soon as the dye is flushed out, the water is virtually free of NaCl. Also, the exit water just prior to a 5000 mg/L NaCl plume breakthrough at the effluent reservoir porous plate had a Na^+ concentration of 6.1 mg/L, showing that the NaCl front did not travel ahead of the dye front.

3.2 Homogeneous Medium

The porosity was first estimated for the homogeneous case by recording the volume of water required to fill the voids in the porous media and end reservoirs, each of which has known dimensions. Another method to determine the in-model porosity is through the relationship between specific discharge, average pore velocity and porosity. A dye front is introduced into the tank, its velocity is measured and knowing the specific discharge the porosity can be calculated. Both of these methods yielded a value of porosity of 0.38. As the packing of spheres with the same diameter and the resulting porosity are independent of the size of the sphere (de Marsily, 1986), the porosity calculated for one size category of glass beads in the tank would be very similar for all size categories.

In order to test the hydraulic characteristics of the flow tank, a full face Rhodamine WT experiment was

run where the entire inlet fluid was 500 mg/L Rhodamine WT. This test was conducted at about the same average linear groundwater velocity as the future experiments (Table 3, experiment #A1-F). During the test a smooth vertical dye front was observed to move across the tank. These results indicate that there were (1) no short circuiting of flow along the top of the tank and (2) no preferred pathways within the porous medium, and (3) that the flow field was uniform and horizontal.

The first group of experimental trials were designed to examine how the pattern of spreading of a dense plume changed as a function of fluid density. Tracers were introduced into the tank varying from 1000 mg/L to 100,000 mg/L NaCl (Table 3). As expected, the extent of sinking increases with the density of the DAPL. An example of this behaviour is observed with a 5000 mg/L NaCl plume (experiment #A10-B, Table 3). The plume trajectory (Figure 7) was such that the plume hit the bottom of the tank after approximately 31 hours. A particularly interesting feature of the plume was the lobe shaped protuberances (gravitational instabilities), evident first along the bottom edges of the plume (Figure 7a) and later within the plume (Figures 7b and 7c). This pattern of enchanced spreading of solute perpendicular to the ambient groundwater flow field results in dilute and

Table 3. Experimental Data for Homogeneous Medium Runs

Experiment Number	NaCl Conc. (mg/L)	ρ_{20} g/cm^3	$D^{20}/_{20}$	Average Specific Discharge (cm/s)	Average Linear Velocity (cm/s)
A1-F	0	0.9983	1.0001	1.20×10^{-4}	3.17×10^{-4}
A2-F	100000	1.0662	1.0681	1.20×10^{-4}	3.15×10^{-4}
A3-F	25000	1.0157	1.0176	1.23×10^{-4}	3.22×10^{-4}
A4-F	2000	0.9997	1.0015	1.26×10^{-4}	3.30×10^{-4}
A5-B	0	0.9983	1.0001	1.14×10^{-4}	3.00×10^{-4}
A6-B	1000	0.9990	1.0008	1.11×10^{-4}	2.92×10^{-4}
A7-B	2000	0.9997	1.0015	1.16×10^{-4}	3.07×10^{-4}
A8-B	2000	0.9997	1.0015	2.17×10^{-4}	5.70×10^{-3}
A9-B	5000	1.0019	1.0037	2.17×10^{-4}	5.70×10^{-3}
A10-B	5000	1.0019	1.0037	1.16×10^{-4}	3.07×10^{-4}
A11-B	10000	1.0053	1.0071	1.24×10^{-4}	3.28×10^{-4}

ρ_{20} = relative density at 20 degrees Celsius, g/cm^3.

$D20/_{20}$ = specific gravity at 20 degrees Celsuis.

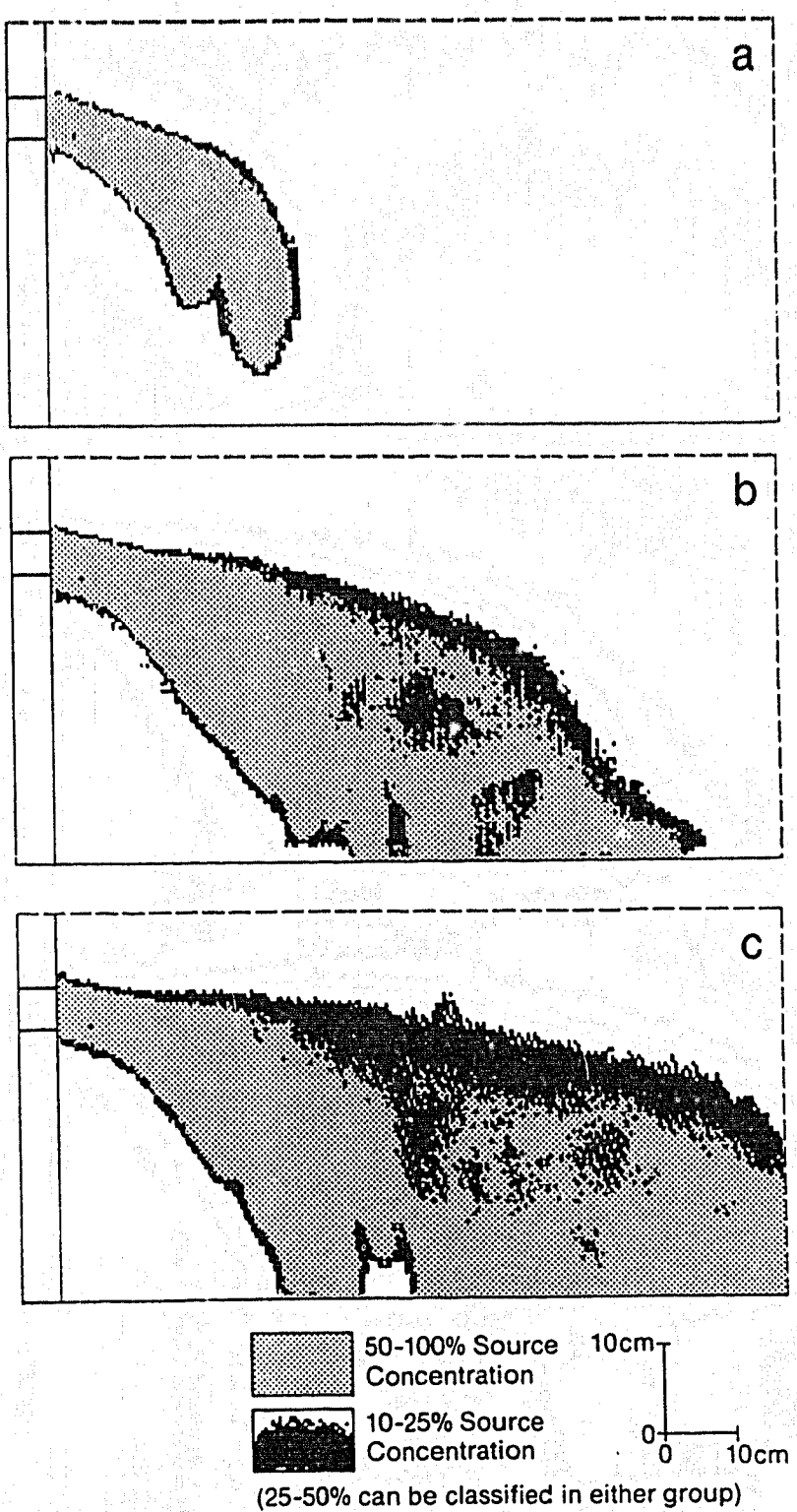

Figure 7. Binary Images for a 5000 mg/L NaCl Source in Homogeneous Medium at Various Times.

concentrated zones within the plume. Also evident is that the highest concentrations of solute occur in the lower portions of the plume while the upper sections are more dilute.

The threshold at which density effects become noticeable in the homogeneous medium experimental trials is about 1000 mg/L. With just the 500 mg/L Rhodamine WT solution, the tracer showed little influence of the Rhodamine WT dye on the transport path and plume trajectory was near horizontal (Figure 8a). With the 1000 mg/L plume, its trajectory was still near horizontal, but the plume became gravitationally unstable and gravity instabilities started to form after approximately 36 hours (Figure 8b). When the solute concentration was raised to 2000 mg/L (Figure 8c) the plume sank to a greater degree, but even after 120 hours, at which time it appeared to be in steady state, the plume did not hit the bottom of the tank. The 10,000 mg/L NaCl plume fell quicker than the 5000 mg/L NaCl plume, hitting the bottom of the tank after only 13 hours.

The character of the gravitational instabilities also depends upon concentration. As the concentration of the tracer increases the gravitational instabilities become more finger shaped, with narrower and longer lobes

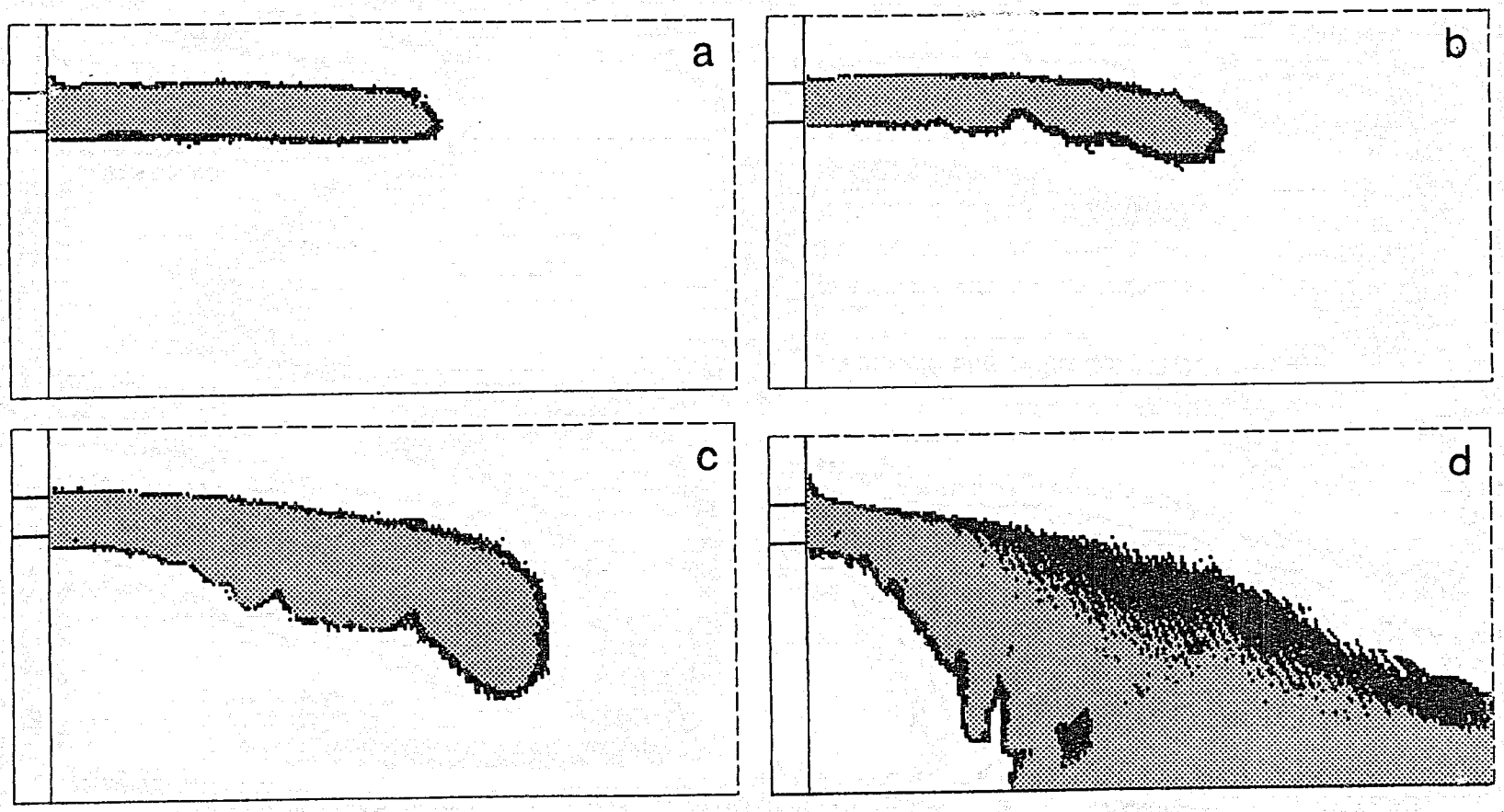

Figure 8. Binary Images for Various Source Concentrations in Homogeneous Medium at 54 Hours. (a) 500 mg/L Rh(WT); (b) 1000 mg/L NaCl; (c) 2000 mg/L NaCl; (d) 10,000 mg/L NaCl

and greater propagation rates (compare Figures 8c and 8d).

The series of plumes in Figure 8 also illustrate how the extent of transverse mass spreading depends upon density and the occurrence of instabilities. The effects are most apparent at plume concentrations greater than 2000 mg/L. As is apparent in Figures 8a and 8b, the 1000 mg/L plume is about the same as the 500 mg/L plume. However, the 2000 mg/L (Figure 8c) is much more vertically disperse than either of these. The spreading is evident in the 50 to 100% high concentration zone, while the more dilute 10 to 25% zone is similar to that of the 500 mg/L plume. At high NaCl concentrations of 25,000 mg/L and 100,000 mg/L, the solutions were sufficiently dense that they flowed out of the injection chamber due to the forces of gravity at a rate greater than tracer was being pumped into the injection chamber. The tracer level within the injection chamber did equilibrate with time, though, so that after 18 hours, for the 100,000 mg/L run, the tracer was being introduced through the lower 1/4 to 1/3 of the injection chamber. These solutions were so dense that they flowed down the porous metal plate and into the lower ambient water injection chamber against the hydraulic gradient. For the 100,000 mg/L NaCl run after 18 hours, the majority of

the plume was diluted to the 10 to 25% concentration level (Figure 9).

As the propagation of density instabilities seems to be an important feature of dense plumes and the resulting transverse dispersion, a time series, with a 2000 mg/L NaCl solution was studied to observe their development (Figure 10). The instabilities require some time before they develop. Once they form, or become visibly evident, they grow in length while being displaced horizontally at the same velocity as the ambient groundwater. They seem at least in the 2000 mg/L NaCl case, to reach quasistable dimensions shortly after their initial development (compare instability shape for t=54 hours, Figure 8, and t=120 hours, Figure 10).

Experiments were also conducted to observe the effect of velocity on plume migration and instability development. In these trials, plumes with concentrations of 2000 mg/L and 5000 mg/L NaCl were developed at a groundwater velocity of 5.70×10^{-3} cm/s (approximately 18 times faster than previous runs, see Table 3). In both cases no instability development occurred. Comparing the plume outlines for the straight 500 mg/L Rhodamine WT and 5000 mg/L NaCl runs (Figure 11), very little difference exists except that whereas the 500 mg/L plume is nearly horizontal, the trajectory of the 5000 mg/L plume is

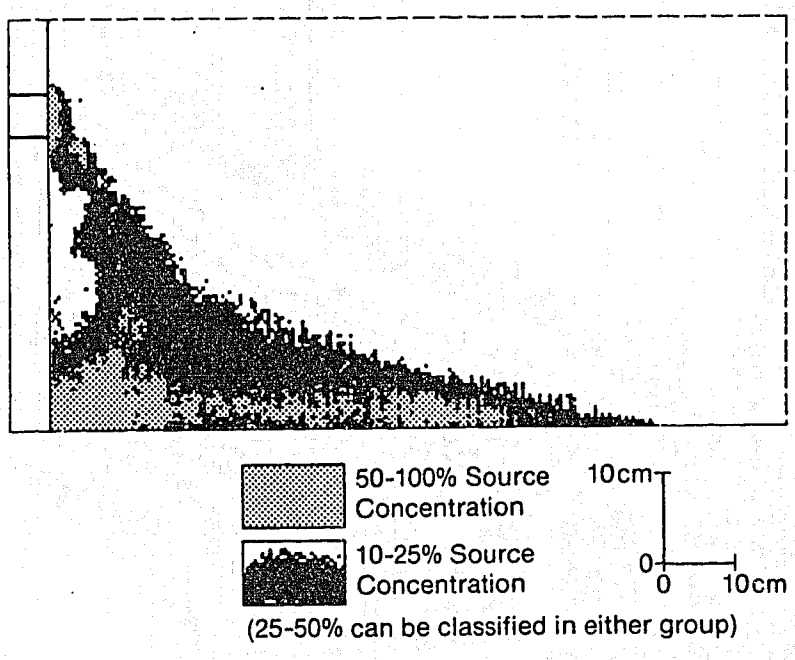

Figure 9. Binary Image for a 100,000 mg/L NaCl Source in Homogeneous Medium at 18 Hours

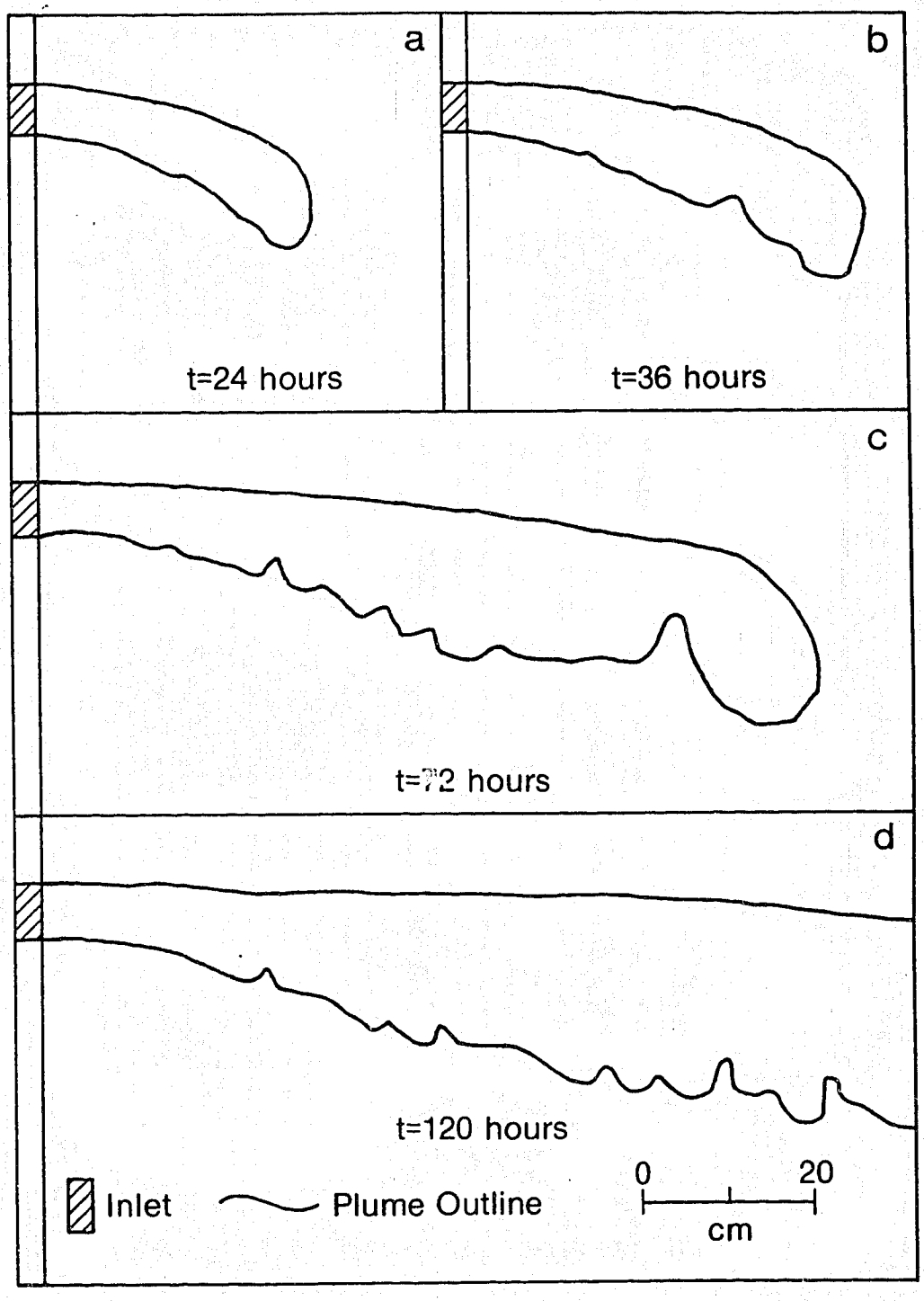

Figure 10. Instability Development Over Time for a 2000 mg/L NaCl Source in Homogeneous Medium. (a) t=24 hours; (b) t=36 hours; (c) t=72 hours; (d) t=120 hours

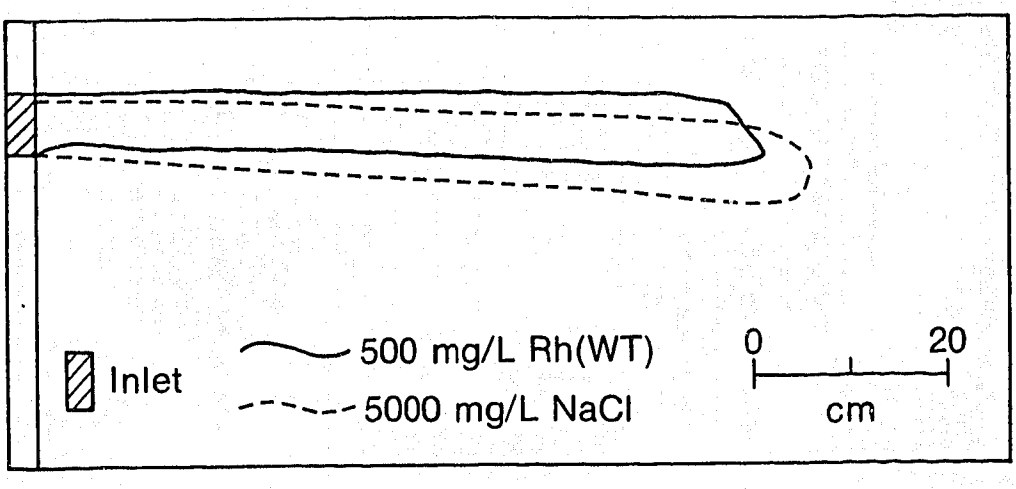

Figure 11. Plume Outlines for 500 mg/L Rh(WT) and 5000 mg/L NaCl (High Velocity) Source in Homogeneous Medium

angled slightly downward. After the velocity was decreased in the middle of the run from 5.70×10^{-3} cm/s to 3.00×10^{-4} cm/s, gravitational instabilities formed. Figure 12 shows the plume outline 12 hours after the change from high to low velocity. The dotted lines refer to instabilities that formed a few grain diameters back from the wall and therefore were lighter in colour than those along the wall. This apparent three-dimensionality of the instabilities was also observed in the previous runs, where the trajectory of the plume at the back and front of the tank were the same at all times but shape and position of the instabilities varied from front to back.

This issue of shape and position of the instabilities was investigated in a run where 2000 mg/L solution (experiment #A7-B) was introduced at near identical conditions to a previous run (experiment #A4-F) to determine how reproducible plume shape and trajectory would be. The two plume outlines at 54 hours (Figure 13) show that while plume trajectories are nearly the same, the size and position of the instabilities are not the same.

3.3 Layered Medium

The following series of experiments was conducted witn the layered medium. The objective was to determine

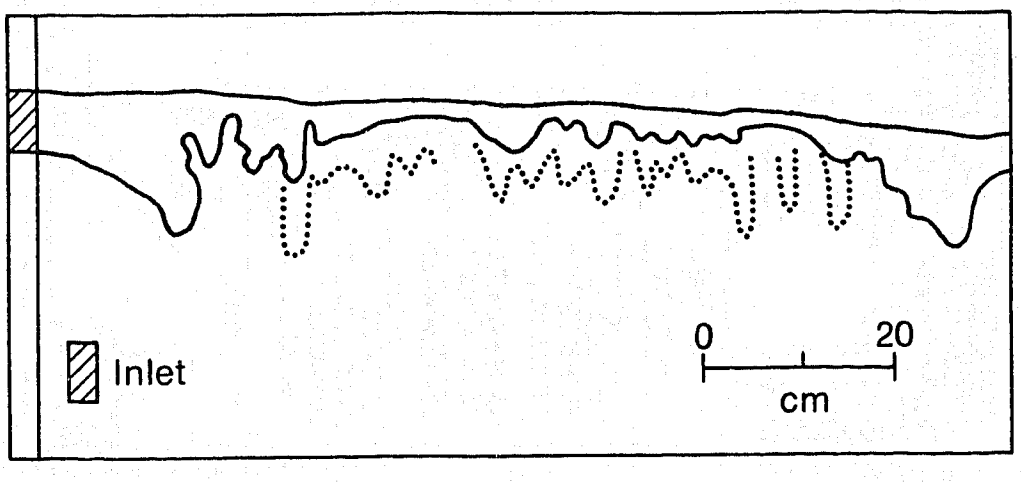

Figure 12. Plume Outline of 5000 mg/L NaCl Source Run in Homogeneous Medium 12 Hours After Velocity Decrease from 5.70×10^{-3} to 3.00×10^{-4} cm/s

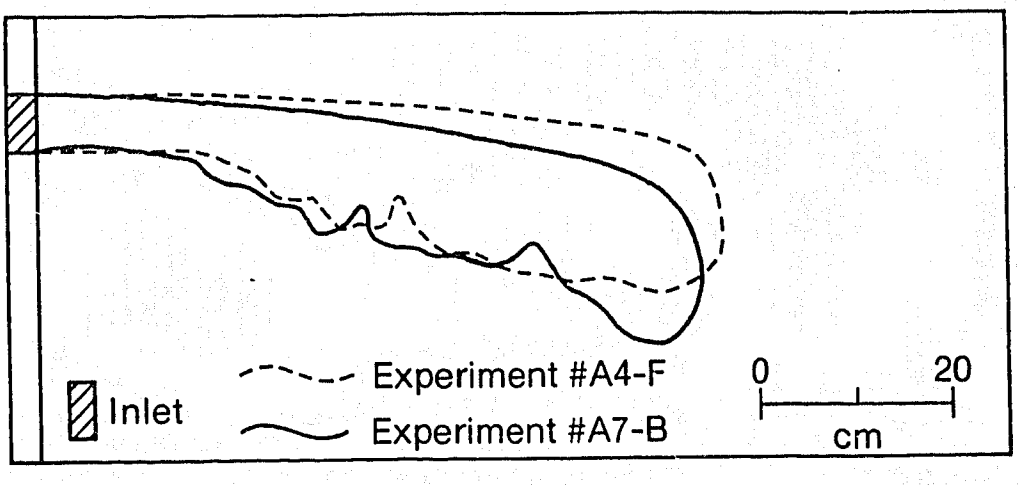

Figure 13. Plume Outlines of Two 2000 mg/L NaCl Plumes at 54 hours

how layers of varying hydraulic conductivity influence plume fall, specifically the way in which the plume trajectory changes as the DAPL interacts with or penetrates layers of progressively lower hydraulic conductivity. Overall, eight trials were run, six with horizontal layers and two with the layers inclined downdip 9 degrees off horizontal (Table 4). The position of the layers and lenses (for lenticular medium) in an image processed plume can be seen in the Appendix, Figure A1.

Rhodamine WT at a concentration of 500 mg/L was introduced along the entire injection width in order to determine the relative average linear groundwater velocity in the various layers. This tracer test, at a given specific discharge, provides the relative groundwater velocity in each of the layers at other values of specific discharge. As can be seen from Table 4, experiments were all run with the average linear velocity in sand layer #5 close to the value for the homogeneous runs. Again, in the layered case, the first group of runs were used to examine how plume shape depended upon density.

When a 2000 mg/L NaCl solution was introduced into the central layer, the plume hit the boundary between the #3 and #5 glass beads at approximately 6 hours. The

Table 4. Average Linear Velocities for Each Layer

Experiment Number	NaCl Conc. (mg/L)	ρ_{20} g/cm^3	$D^{20}/20$	Average Specific Discharge (cm/s)	Average Linear Velocity (cm/s)
B1-B	0	0.9983	1.0001	1.16×10^{-4}	#3 1.30×10^{-3} #5 2.60×10^{-4} #7 1.55×10^{-4} #10 6.73×10^{-5} #13 2.17×10^{-5}
B2-B	0	0.9983	1.0001	1.35×10^{-4}	#3 1.51×10^{-3} #5 3.02×10^{-4} #7 1.77×10^{-4} #10 7.80×10^{-5} #13 2.52×10^{-5}
B3-B	2000	0.9997	1.0015	1.39×10^{-4}	#3 1.56×10^{-3} #5 3.10×10^{-4} #7 1.82×10^{-4} #10 8.05×10^{-5} #13 2.58×10^{-5}
B4-B	5000	1.0019	1.0037	1.38×10^{-4}	#3 1.55×10^{-3} #5 3.10×10^{-4} #7 1.82×10^{-4} #10 8.02×10^{-5} #13 2.58×10^{-5}
B5-B	10000	1.0053	1.0071	1.38×10^{-4}	#3 1.55×10^{-3} #5 3.10×10^{-4} #7 1.82×10^{-4} #10 8.02×10^{-5} #13 2.58×10^{-5}
B6-BT	10000	1.0053	1.0071	1.40×10^{-4}	#3 1.57×10^{-3} #5 3.13×10^{-4} #7 1.83×10^{-4} #10 8.13×10^{-5} #13 2.62×10^{-5}
B7-BT	25000	1.0157	1.0176	1.39×10^{-4}	#3 1.56×10^{-3} #5 3.10×10^{-4} #7 1.82×10^{-4} #10 8.05×10^{-5} #13 2.58×10^{-5}
B8-B	25000	1.0157	1.0176	1.38×10^{-4}	#3 1.55×10^{-3} #5 3.08×10^{-4} #7 1.80×10^{-4} #10 7.98×10^{-5} #13 2.57×10^{-5}

ρ_{20} = relative density at 20 degrees Celcius, g/cm^3.
$D20/_{20}$ = specific gravity at 20 degrees Celcius.

plume advanced along the #3, #5 interface but apparently did not penetrate it. The 5000 mg/L NaCl solution hit the #3, #5 boundary after only one hour and moved along the #3, #5 interface much as the 2000 mg/L solution but the plume did begin to penetrate the interface (Figure 14a). After 18 hours the DAPL had penetrated fairly evenly, approximately 1.5 cm, into the #5 layer. This pattern of vertical spreading then changed as the plume advanced downward into the #5 layer in the form of 3 or 4 major lobes or instabilities (Figure 14b). These lobes penetrated the lower hydraulic conductivity layer and moved horizontally at the particular groundwater velocity for that layer. Figures 14c and 14d show how the layers have inhibited plume fall where the tracer has mounded or collected on the #5, #7 interface in some locations. It should be noted that although the tracer penetrating the #7 layer shows up on the lower concentration binary image, this is probably a full strength tracer penetrating in the form of an instability a few grain diameters inward of the tank wall.

A similar pattern of plume migration is observed for the 10,000 mg/L NaCl solution, but instability development and penetration of layers occurred to deeper levels and more rapidly (Figures 15a and 15b). With the increased density, the plume penetrated deeper, but the

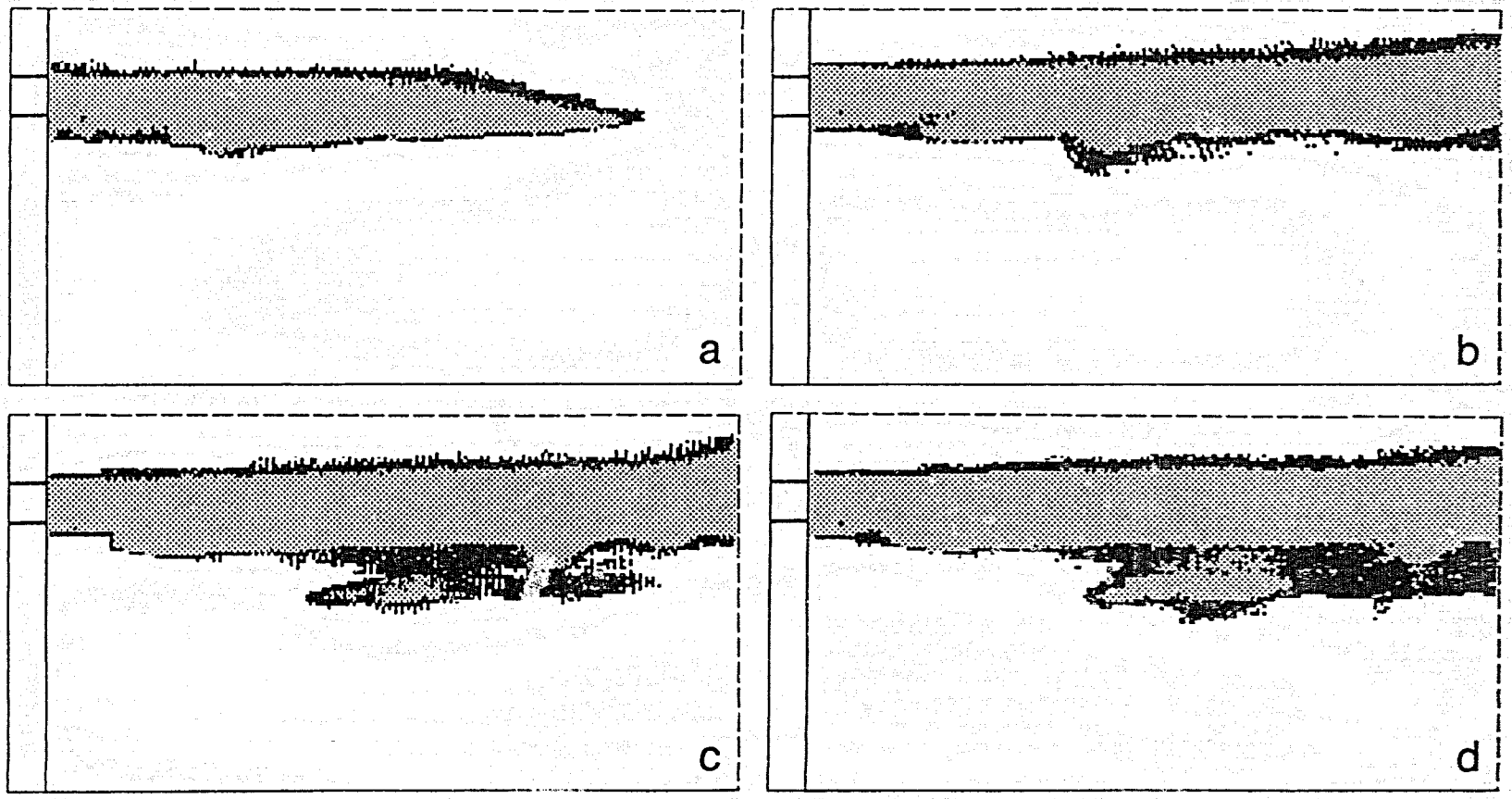

Figure 14. Binary Images for [illegible] mg/L NaCl Source in Layered [illegible] at Various times. (a) t=12 hours; (b) t=24 hours (c) t=54 hours (d) t=[illegible] hours

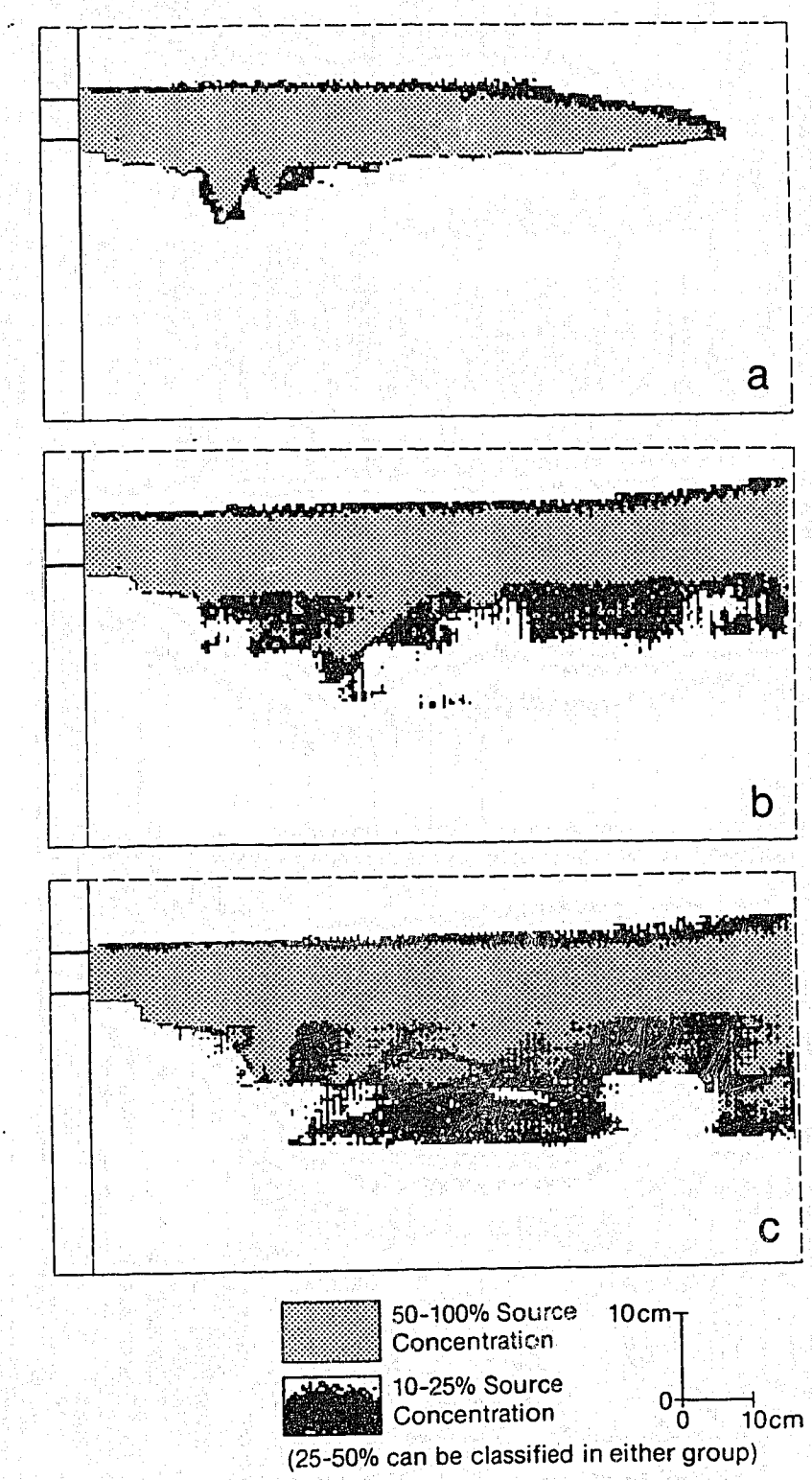

Figure 15. Binary Images for a 10,000 mg/L NaCl Source in Layered Medium at Various Times. (a) t=12 hours; (b) t=48 hours; (c) t=72 hours

#7, #10 interface again seemed to act as a barrier for this particular plume density. Interface contact was made at approximately 48 hours but after 72 hours the #7, #10 interface has not yet been convectively penetrated (Figure 15c).

When the advance of the dye front at various concentrations is compared with the advance of just the 500 mg/L Rhodamine WT dye front, it is evident that as concentration (density) increases, the plume front travels progressively faster than the ambient groundwater velocity. Figure 16a to 16e show the plume outlines for horizontal strata and when the slightly different ambient velocities of each run are taken into account (Table 5), the plume migration velocities were as high as 34% greater than ambient groundwater velocity. However, the decrease in velocities as calculated at 3, 6, and 12 hours shows that this is due mainly to the redistribution of mass in a more gravitationally stable wedge shaped front. When the strata were inclined downdip nine degrees, the effect of gravity on the plume was to increase plume velocity by a little more than 10% for the 25,000 mg/L NaCl solution (Figure 16f and Table 5). The nine degree dip also caused a more even penetration of the #3, #5 interface with the plume advancing deeper over a greater horizontal distance.

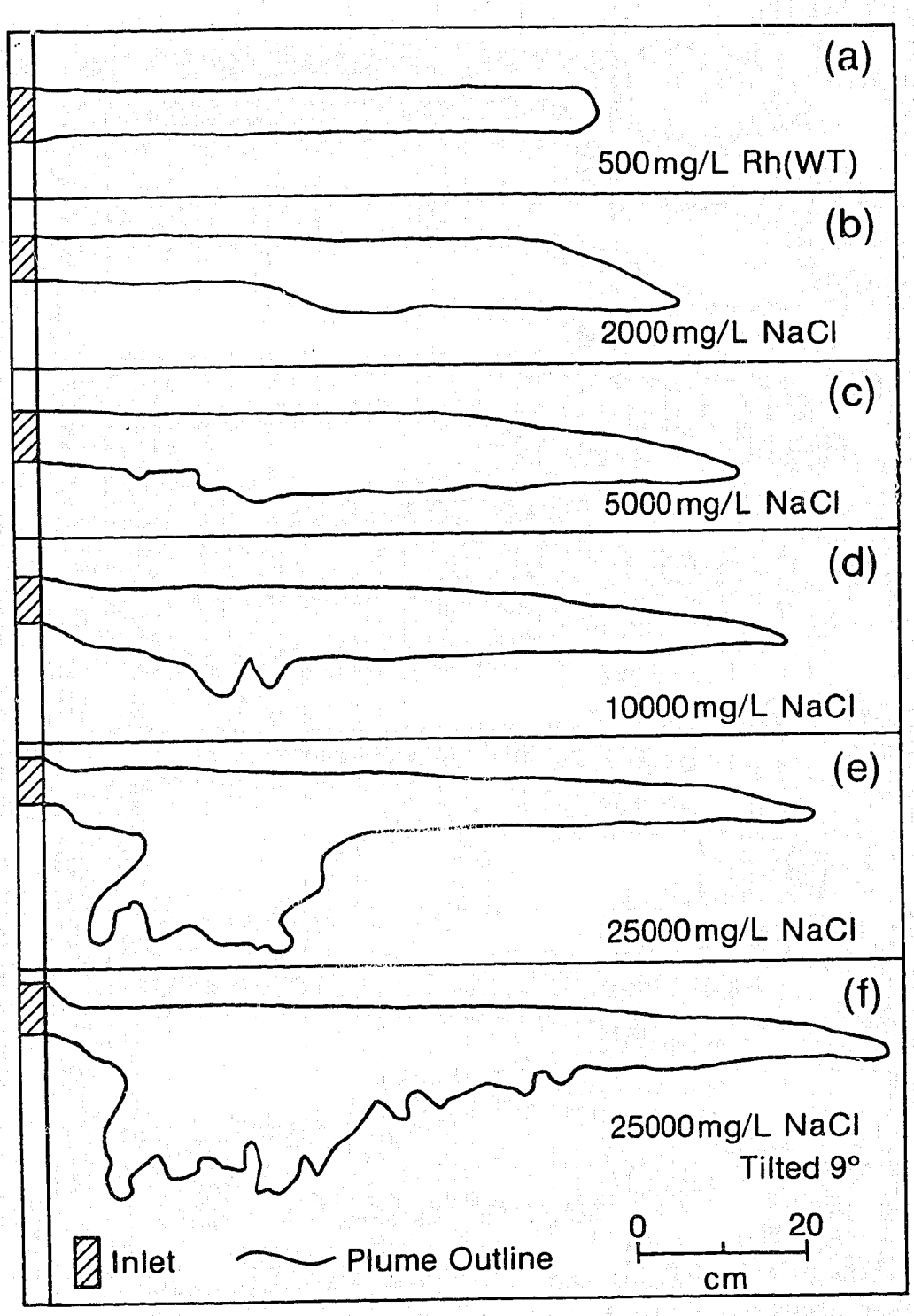

Figure 16. Plume Outlines for Various Source Concentrations in Layered Medium at t=12 hours. (a) 500 mg/L Rh(WT); (b) 2000 mg/L NaCl; (c) 5000 mg/L NaCl; (d) 10,000 mg/L NaCl; (e) 25,000 mg/L NaCl; (f) 25,000 mg/L NaCl (9 degree dip)

Table 5. Horizontal versus Inclined Strata Plume Velocities

Experiment Number	NaCl Conc. (mg/L)	Actual Plume Velocity (cm/s)	Average Linear Velocity (cm/s)	Percent Difference in Velocity based on 12 hours
B2-B	0	1.51×10^{-3} (8hrs.)	1.51×10^{-3}	0%
B3-B	2000	1.65×10^{-3} (4hrs.)	1.56×10^{-3}	
		1.70×10^{-3} (6hrs.)		
		1.72×10^{-3} (12hrs.)		10%
B4-B	5000	2.18×10^{-3} (3hrs.)	1.55×10^{-3}	
		2.02×10^{-3} (6hrs.)		
		1.88×10^{-3} (12hrs.)		21%
B5-B	10000	2.48×10^{-3} (3hrs.)	1.55×10^{-3}	
		2.27×10^{-3} (6hrs.)		
		2.02×10^{-3} (12hrs.)		30%
B6-BT	10000	2.62×10^{-3} (3hrs.)	1.57×10^{-3}	
		2.37×10^{-3} (6hrs.)		
		2.15×10^{-3} (12hrs.)		37%
B7-BT	25000	3.22×10^{-3} (3hrs.)	1.56×10^{-3}	
		2.68×10^{-3} (6hrs.)		
		2.28×10^{-3} (12hrs.)		46%
B8-B	25000	2.85×10^{-3} (3hrs.)	1.55×10^{-3}	
		2.42×10^{-3} (6hrs.)		
		2.08×10^{-3} (12hrs.)		34%

3.4 Lenticular Medium

The last series of experimental runs was conducted with a lenticular medium. Again, the objective of these runs was to describe how plume spreading depends on the interaction of the DAPL with the heterogeneous porous medium. Overall, five trials were run with fluids ranging in density from 2000 to 25,000 mg/L NaCl (Table 6). In Table 6, the average linear velocity is based solely on an average porosity of 0.38 and does not take into account the widely differing velocities within the lenses. The base case again involved running a 500 mg/L Rhodamine WT tracer. The plume shape, depicted in Figure 17a at 72 hours, clearly shows how spreading was much more complex than for either the cases of the layered or homogeneous media. The plume width has decreased close to the source because of a high hydraulic conductivity lens (size #3 glass beads). Upon leaving the first high conductivity lens the tracer has spread upward toward another #3 lens and downward and around a #7 low conductivity lens. The influence that high conductivity lenses can exert is also seen as the upper #3 lens near the exit reservoir has pulled the DAPL up, in a diluted form, right through a #7 low conductivity lens (Figure 17b).

Table 6. Experimental Data for Lenticular Medium Runs

Experiment Number	NaCl Conc. (mg/L)	ρ_{20} g/cm3	D20/20	Average Specific Discharge (cm/s)	Average Linear Velocity (cm/s)
C1-B	0	0.9983	1.0001	1.17x10-4	3.08x10-4
C2-B	2000	0.9997	1.0015	1.05x10-4	2.77x10-4
C3-B	5000	1.0019	1.0037	1.09x10-4	2.87x10-4
C4-B	10000	1.0053	1.0071	1.10x10-4	2.90x10-4
C5-B	25000	1.0157	1.0176	1.18x10-4	3.10x10-4

ρ_{20} = relative density at 20 degrees Celsius, g/cm3.

D20/20 = specific gravity at 20 degrees Celsius.

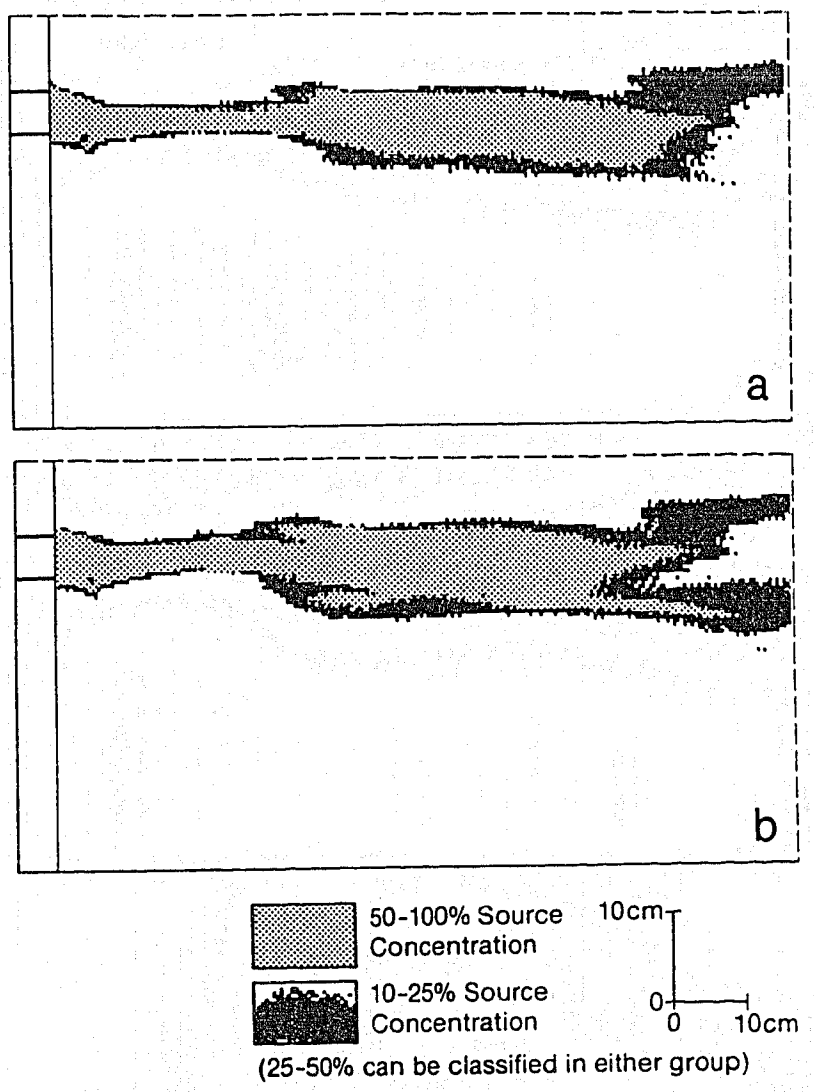

Figure 17. Binary Images for Various Source Concentrations in Lenticular Medium at t=72 Hours. (a) 500 mg/L Rh(WT); (b) 2000 mg/L NaCl

For the 2000 mg/L plume, it is apparent the lenses acted to inhibit plume fall and instability development. The 2000 mg/L NaCl plume (Figure 17b) was similar to the 500 mg/L Rhodamine WT plume (Figure 17a), except that the 2000 mg/L plume fell somewhat and occupied part of the #3 lens below the center tie rod, a lens that in the 500 mg/L Rhodamine WT run only had ambient water flowing through it.

When the density was increased to 1.0019 g/cm^3 (5000 mg/L NaCl), the plume bifurcated, with the lower section falling through the #7 lens near the injection zone and being carried into the #3 lens directly below the #7 lens (Figure 18a). The plume later evolved (Figure 18b) with three leading fronts as the combination of low and high conductivity lenses split up the plume. Instability development has been inhibited and is less predictable, and convectively falling fingers have been pulled into high conductivity lenses or dispersed by low conductivity lenses, giving way to a diverse plume geometry (Figures 18b and 18c). Comparisons of early and later distribution show that the entire plume is changing shape in a transient manner. For example, the binary images for t=96 hours (Figure 18d) indicate that the large instability lobe near the source that developed after 24 hours was growing and would probably have bifuracted the

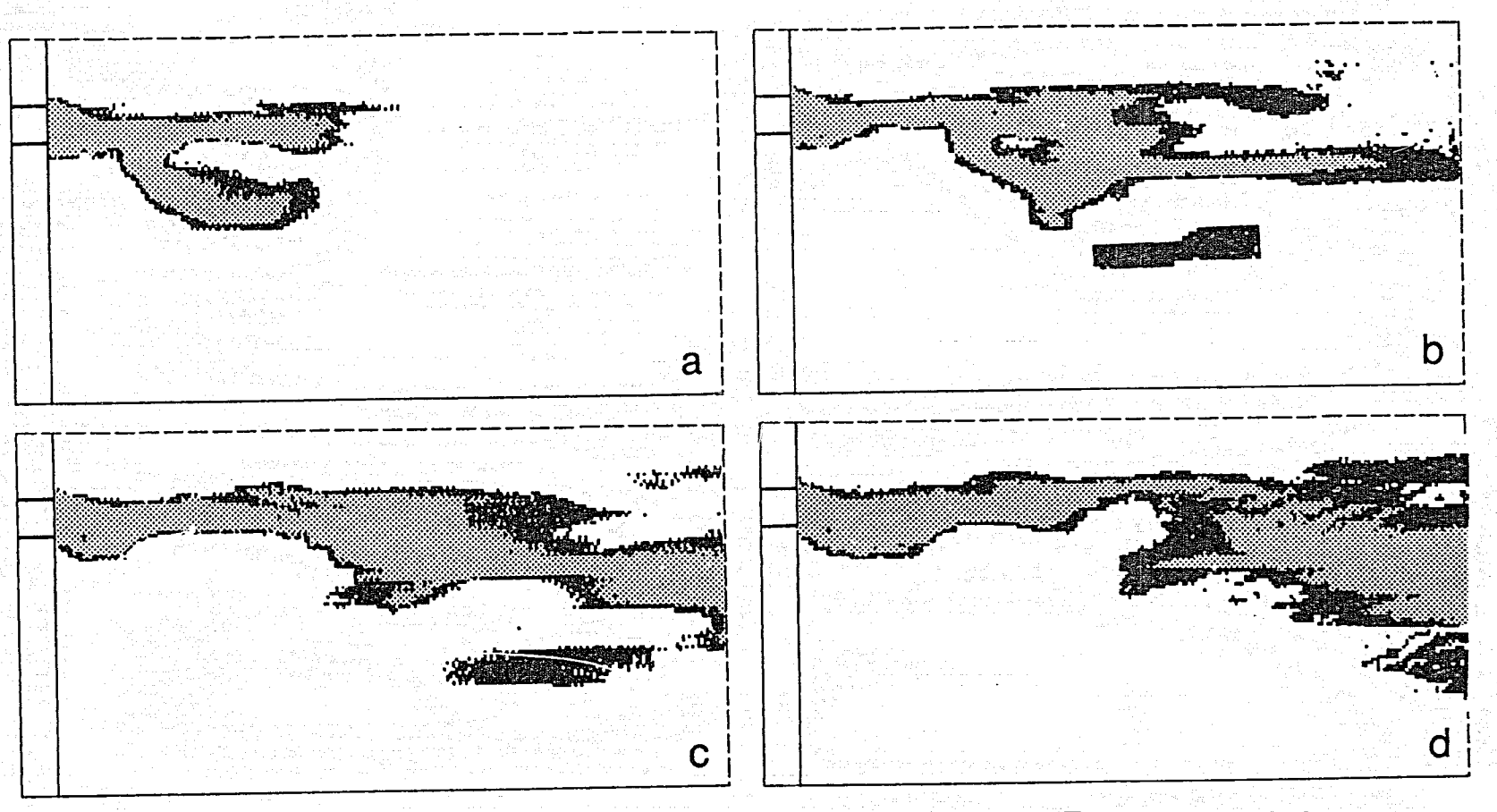

Figure 18. Binary Images for a 5000 mg/L NaCl Source in Lenticular Medium at Various Times. (a) t=24 hours; (b) t=48 hours (c) t=72 hours; (d) t=96 hours

plume at the source again if the run had been left to continue. These transient changes generally illustrate how unpredictable plume shape might be even in places through which the DAPL has already flowed.

When the concentration was increased to 10,000 mg/L, the plume fall was much more rapid, and bifurcation and subsequent three way splitting of the plume occurred much earlier. Also, as was observed in the 25,000 mg/L run in the layered media experiments, the low conductivity lenses did not seem to retard plume fall as effectively as they did in the 2000 and 5000 mg/L experiments. After 48 hours (Figure 19) the classic instability development and shape can be seen again as in the homogeneous medium: small lobes along the lower upgradient portion of the plume. Also, the high concentration zones have not been limited to the lower portions of the plume but also occur along high conductivity flow paths (Figure 19b). Still, the lenses did act to retard plume fall. During the 5000 mg/L NaCl run the plume did not hit the bottom of the tank, but with a density increase up to 1.0053 g/cm^3 (10,000 mg/L NaCl), the plume hit bottom after about 87 hours. This result is in marked contrast to the homogeneous runs, where the 10,000 mg/L plume hit bottom after about 13 hours. The lenses also dispersed the plume to a greater extent than was observed in either the

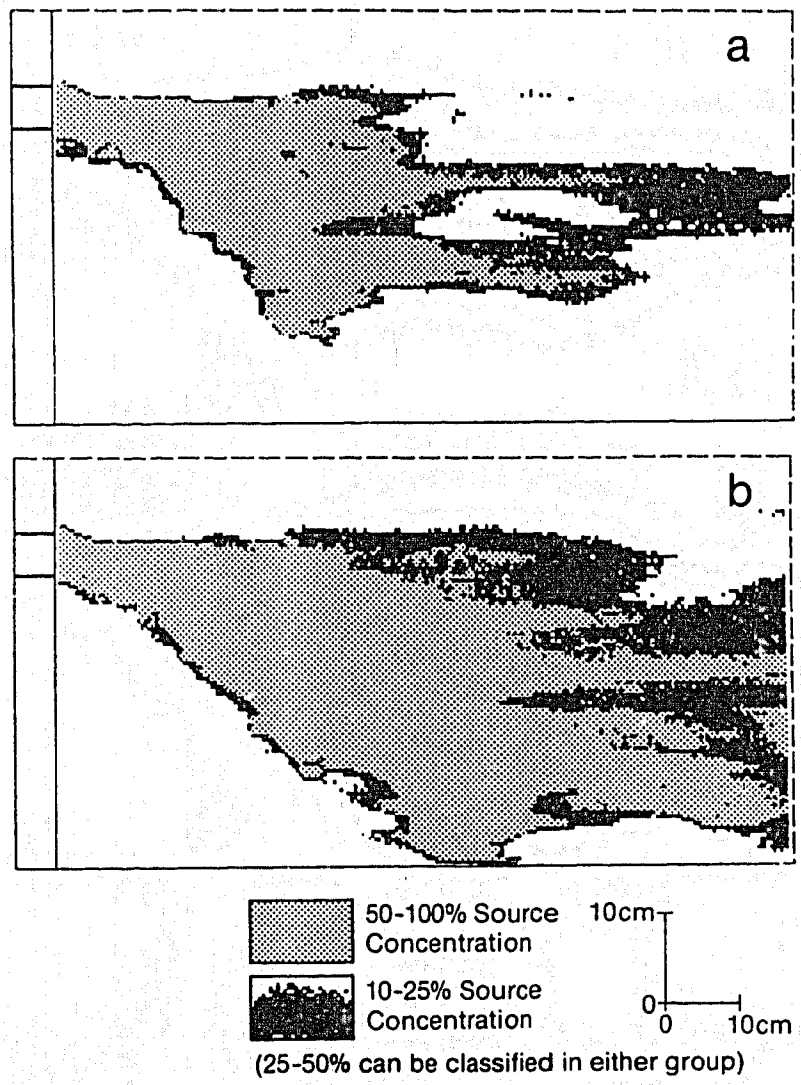

Figure 19. Binary Images for a 10,000 mg/L NaCl Source in Lenticular Medium at Various Times. (a) t=48 hours (b) t=96 hours

homogeneous or layered cases, in that high conductivity pathways could move the tracer at higher concentrations in the upper portions of the plume. With a 25,000 mg/L NaCl solution the plume hit the bottom of the tank after approximately 29 hours. After 72 hours the plume was dispersed over almost the entire tank (below injection chamber) and was too dilute to isolate it from the background error on the image analysis computer.

4. DISCUSSION

The realization that dense plumes sink is inherent in the basic physical laws of groundwater flow. The equation for velocity as described by (Davies, 1987),

$$\vec{V}_R = -K \left[\text{grad } h + \frac{\Delta \rho}{\rho} \right] \qquad (4.1)$$

$\vec{V}_R$ = resultant velocity vector (L/T)
K = hydraulic conductivity (L/T)
grad h = gradient of hydraulic head
$\Delta \rho$ = difference between plume density and ambient groundwater density
ρ = density of ambient groundwater

provides a simple starting point to determine if a plume will sink in homogeneous isotropic media but its applicability is otherwise limited. This form of the equation is simply the vector sum of the forces that act on a given fluid element (Figure 20), and thus does not take into account dispersion and changing plume density. When applied to the homogeneous experiments, this conceptualization fairly accurately predicts the overall character of plume behaviour. As shown in Table 7, calculations of $\vec{v}$ and $\vec{u}$ for the 500 mg/L Rhodamine WT tracer solution are 5.6×10^{-6} cm/s and 3.0×10^{-4} cm/s, respectively. Because the horizontal ambient groundwater

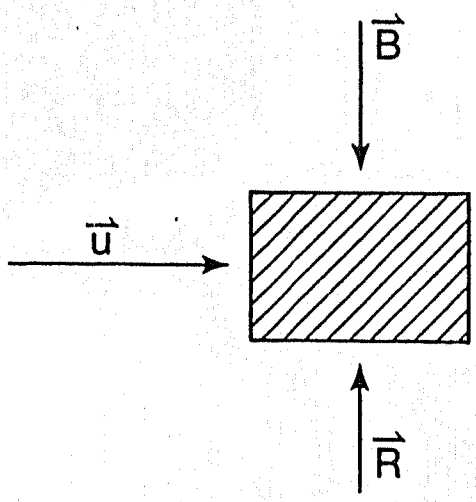

$\vec{B}$ = Vertical driving force on the fluid element; for hydrostatic conditions it equals the difference in weight between the fluid and the ambient fluid displaced.

$\vec{R}$ = vertical resisting force on fluid as it passes through the porous medium.

$\vec{u}$ = ambient groundwater velocity = -K grad h

$$\vec{B}+\vec{R} = -K\frac{\Delta\rho}{\rho} = \vec{v}$$

Figure 20. Forces That Act on a Given Fluid Element
(modified from Paschke, 1982)

Table 7. Calculation of $\vec{v}$ and $\vec{v}_R$ for Various Homogeneous Medium Experiments

Experiment Number	NaCl Conc. (mg/L)	ρ_{20} g/cm^3	$\vec{u}$(cm/s)	$\vec{v}$(cm/s)	Trajectory Angle ($\vec{v}_R$, degrees)**
A5-B	0	0.9983	3.00×10^{-4}	$v = -K\frac{\Delta\rho}{\rho}$. $=5.6\times10^{-6}$	1
A6-B	1000	0.9990	2.92×10^{-4}	4.5×10^{-5}	9
A7-B	2000	0.9997	3.07×10^{-4}	8.4×10^{-5}	15
A9-B	5000	1.0019	5.70×10^{-3}	2.1×10^{-4}	2
A10-B	5000	1.0019	3.07×10^{-4}	2.1×10^{-4}	34

ρ_{20} = relative density at 20 degrees Celsius, g/cm^3.

$K = 5.6\times10^{-6}$ cm/s

** 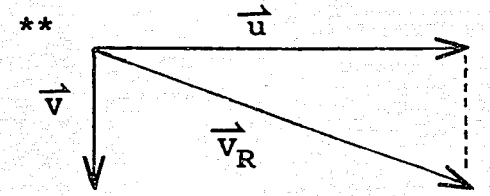

flow vector greatly exceeds the vertical density dependent vector, flow is nearly horizontal, as observed in Figure 8a. Similar calculations are presented in Table 7 for the 1000, 2000 and 5000 mg/L NaCl tracers. Comparing some of the calculated results to the observed plume trajectories (prior to the plume hitting the bottom of the tanks, Figures 8b, 8c and 7a) shows that the simple calculation does indeed enable calculation of the approximate plume trajectory. Thus, vector resolution provides a means to estimate if density dependent flow will be important in a given situation provided we can assume our porous medium (site stratigraphy) is isotropic and homogeneous.

Because the rate at which a fluid element sinks is independent of the ambient velocity, it is possible to run sand tank experiments at such a high velocity that density effects appear negligible. For example, compare the plume trajectories for experiments #A9-B and #A10-B (Table 7). When the ambient groundwater velocity is 5.7×10^{-3} cm/s, the plume will sink at a trajectory angle of about 2 degrees, as compared to 34 degrees when $\vec{u}$ is 3.0×10^{-4} cm/s. Examples exist in the literature (e.g., Paschke and Hoopes, 1984) for which unrealistically high flow velocities in tank experiments have masked density effects.

The simple theory just described does not account for the vertical mixing due to density effects. Results from experiments with the homogeneous medium demonstrates how vertical dispersion is enhanced by density-related effects. This contribution to the overall transverse dispersion can be referred to as "convective dispersion" because it originates not from mechanical mixing (mixing in individual pores and pore channels) during fluid advection, but due to fluid convection. The term convection implies the motion of fluid due to buoyancy effects, be they thermal or solute-density induced. In the homogeneous medium experiments, spreading related to classical diffusion and mechanical dispersion played a small role in the overall dispersion process as is evidenced by the small zone of dispersion developed within the Rhodamine WT tracer test (Figure 8a).

The relative importance of diffusion and mechanical dispersion in the dispersion process can be defined by values for the effective diffusion coefficient (D'_d) and the coefficient of hydrodynamic dispersion (D). From these two coefficients, the coefficient of mechanical dispersion (D') can be deduced from the following relation

$$D=D'+D'_d \qquad (4.2)$$

James and Rubin (1972), in their laboratory dispersion study involving a column packed to a porosity of 0.35 with 250 to 500 micron glass beads, found longitudinal hydrodynamic dispersion values at three different velocities (Table 8). The column study of De Smedt and Wierenga (1984) used smaller glass beads, 74-125 microns, but came up with similar values to those of James and Rubin (1972). These studies verify the accepted notion that microscale effects by themselves do not create significant mixing in laboratory studies with homogeneous media.

The free solution diffusion coefficient, D*, for dilute NaCl solution is 1.61×10^{-5} cm^2/s at 25 degrees Celsius (Robinson and Stokes, 1970). One relationship for the effective diffusion coefficient, D'_d, for nonsorbed species in porous media is given by the relation

$$D'_d = \tau D^* \qquad (4.3)$$

where τ is the tortuosity of the porous medium, which takes into account the longer paths of diffusion caused by the presence of the porous medium (Bear, 1972). Using a typical value for sands of $\tau = 0.7$ (de Marsily, 1986) gives a $D'_d = 1.13 \times 10^{-5}$ cm^2/s. This estimate corresponds

Table 8. Hydrodynamic Dispersion Coefficients

Researcher	Porous Media Size (mm)	Average Linear Velocity (cm/s)	Hydrodynamic Dispersion Coefficient ($cm^2/s.$)
James and Rubin (1972)	0.25-0.50	8.73×10^{-5} 4.88×10^{-4} 3.03×10^{-3}	1.0×10^{-5} 1.22×10^{-5} 4.2×10^{-5}
De Smedt and Weirenga (1984)	0.074-0.125	4.67×10^{-4}	3.24×10^{-5}

fairly well with De Smedt and Wierenga's value for D'_d of $1.00x10^{-5}cm^2/s$ for a $CaCl_2$ solution in their study of solute transfer through columns of glass beads.

Using a value of $1.22x10^{-5}$ cm^2/s (Table 8) for the coefficient of hydrodynamic dispersion that corresponds most closely to our homogeneous experiments both in media and velocity, and a value of $1.13x10^{-5}$ cm^2/s for D'_d, we obtain a value of $9.00x10^{-7}$ cm^2/s for D'. This calculation indicates that at least in the homogeneous experiments mechanical dispersion plays a very small role in the dispersion process.

The process of convective dispersion appears to include two components, an overall spreading because the mean density of the plume is larger than the ambient groundwater, and more localized spreading due to the development of gravitational instabilities. The first effect appears to cause significant transverse dispersion. The simple observation in Figure 8 that the spreading from the denser plume is greater than the less dense one confirms this conclusion. In any case, where instabilities develop, spreading is enhanced to an even greater extent.

The development of gravity instabilities is a process of gravitational free convection of the plume. They develop when more dense fluids occur above less

dense fluids in a configuration that is inherently unstable. The development of instabilities can be explained as follows. The curvature of the microscopic boundaries in the porous media between displacing and displaced fluid (due to a distribution of pore sizes, combined with molecular diffusion and dispersion of the solute) induces a macroscopic rotation of the plume - ambient water interface (Bachmat, 1969). As this interface is gravitationally unstable this rotation/mixing of the interface is a means of bringing the system into equilibrium.

Studies explaining gravitational phenomena in porous media are extremely limited. Bachmat (1969) and Bachmat and Elrick (1970) studied these gravity instabilities both theoretically and experimentally for the case of miscible fluids in a vertical porous column in the absence of any ambient flow field. They included this phenomenon of solute spreading as part of the dispersion process and referred to it as convective dispersion. An important feature of these instabilities, as the experiments showed, is their tendency to depend on several interrelated factors including density and groundwater velocity. Instabilities may not develop for a relatively dense fluid if it moves much faster than $\vec{v}$. this is the reason why in experiments #A9-B and #A10-B

instabilities were observed in the 5000 mg/L plume, where $\vec{u}=3.07\text{x}10^{-4}$ cm/s, but not in experiment #A9-B, where $\vec{u}=5.70\text{x}10^{-3}$ cm/s. Overall, my experience with these instabilities has been not unlike that observed generally for problems of fluid mechanics. Their development is a balance between the effects of viscosity, gravity, pore size and distribution, diffusion and velocity. What needs to be emphasized is that the development of instabilities is an integral part of the convective dispersion of DAPLs. When convective dispersion occurs it is by density segregation and the propagation of instabilities.

Dispersion and diffusion have a dampening effect on the observation of these instabilities, as they widen the transition region and effectively smear out some of the small instabilities in the interfacial region before they have a chance to grow (Coskuner and Bentsen, 1987). Pore size influences instability development and propagation in that the coarser the material, the faster the convective dispersion or instability propagation (Bachmat and Elrick, 1970). In experiments with fine size glass beads (29 microns average diameter, $K=7.2\text{x}10^{-4}$ cm/s), Bachmat and Elrick (1970) did not observe any hydrodynamic instabilities even for a 55,500 mg/L $CaCl_2$ solution, whereas instability development was prevalent

in glass beads with an average diameter of 100 microns ($K=1.1x10^{-2}$ cm/s) and a 27,750 mg/L $CaCl_2$ solution. The higher the velocity, the smaller typically are the dimensions of the instability (R.G. Bentsen, personal communication, 1988). Therefore, the instabilities may be small enough that they are not observed.

The forces of viscosity also serve to dampen the development of instabilities in a miscible system (Wooding, 1959), as opposed to the more commonly dealt with immiscible fluids, where the forces of viscosity tend to render the system unstable if the displacement velocity is large enough.

The mean plume trajectories in many cases were the same, as evidenced by similar plume geometries on the front side and backside of the tank. Gravity instabilities, however, are three dimensional features so that tracer distributions observed along the tank wall may not be the same in the center of the tank or along the opposite wall. Bachmat and Elrick (1970) observed this effect in their column work and it was evident in this study.

The influence on the flowlines within the tank due to the instability development should not be a global effect, as these instabilities form, according to Polivanova (1971), with the denser fluid moving downwards

and the lighter fluid moving upwards. Therefore, as far as the flowlines are concerned, the instabilities should cause only very local changes (R.G. Bentsen, personal communication, 1988).

Experiments with homogeneous media suggest that plume fall due to density differences is propagated dominately via instability development, although equation (4.1), which describes the macroscopic or overall plume trajectory, suggests that the instabilities are just perturbations to the general trajectory. Generally, the greater the density difference, the greater the number of fingers propagated per unit length, the greater the rate of propagation and thus the greater the rate of plume fall. Once the plume hits the bottom of the tank, or an impervious boundary, it advances forward, disperses and flows more in the upper portions of the tank as the underlying fluid increases in density and influences incoming tracer fall. Density instabilities continue to form both along the edges and within the plume giving way to high and low concentration zones within the plume. The highest concentrations of solute occur in the lower portions of the plume, while the upper sections are much more dilute (Figure 8d). The experiments also show how easily instabilities can form and the massive vertical convective dispersion that can occur with dense plumes.

However, in reality, a true homogeneous medium as investigated in section 3.2 does not exits. Even those aquifers which are relatively homogeneous when viewed on a large scale, such as the contaminated aquifer at Canadian Forces Base Borden, Ontario, are actually very heterogeneous due to complex distributions of beds and lenses of fine to coarse sand and silt (MacFarlane et al., 1983, and Sudicky, 1986). The layered and lenticular media experiments show how small changes in hydraulic conductivity can drastically change the dispersion process with dense plumes.

The way in which the layers inhibit plume fall for a particular bedding interface (hydraulic conductivity difference) cannot simply be explained with equation (4.1). A reduction in hydraulic conductivity by one order of magnitude across a bedding interface reduces the vertical buoyancy driven velocity component by an order of magnitude but the horizontal ambient groundwater velocity in that layer is also reduced by the same amount. A feature of convective dispersion in layered media is the tendency for mass apparently to mound above the boundary with a low conductivity unit. This effect is illustrated in Figure 14c and 14d, for example, where the DAPL collects on the #7, #10 interface. In this respect, the behaviour of DAPL is not unlike that of a

dense nonaqueous phase organic liquid. However, the reason why this mounding occurs is different. In the case of the DAPL the collection of tracer on a given layer is due to a lack of continuity in mass flow across the horizontal boundary. In this case mass (tracer) is being supplied to the boundary faster than it can move into the layer below it, which has a lower hydraulic conductivity. Therefore we have mass buildup and a visual lack of layer penetration. This mass buildup also results in the redistribution of mass along a given interface in a more gravitationally stable form which effectively throws the plume ahead of the advective front (Figure 16).

Gravitational instability propagation as a mechanism of plume fall and dilution still exists in a layered medium although the instability lobes on the bottom edges of the plumes (Figures 14b, c and d) have different dimensions in comparison to the same plume in a homogeneous medium (Figure 7). Again, as concentration increases, the instabilities are narrower and propagate faster (Figure 15a). The three dimensionality of the instabilities results in an extremely disperse plume, with the low concentration zones probably representing a combination of instabilities forming a few grain

diameters in from the tank wall and later mixing and plume dilution (Figures 15b and 15c).

In the most realistic case of a natural "homogeneous" setting, the lenticular medium, experiments have shown how the flow field adjustment due to a varying hydraulic conductivity distribution influences the gravitational forces of dense plumes. At low concentrations, such as 2000 mg/L NaCl, the vertical driving force due to plume density is overcome by the focusing effect of high conductivity lenses and the dispersing effect of low conductivity lenses so that little difference exists between the 500 mg/L Rhodamine WT plume and the 2000 mg/L NaCl plume (Figure 17). As the plume density increases, instability development and plume fall are masked in comparison to the homogeneous medium, but instabilities still manifest themselves, resulting in disperse and unsteady-state plume geometries (Figure 18). At a certain point, in this study shown by the 10,000 mg/L NaCl plume, gravitational forces overpower the forces of flow redirection due to the lenses and plume migration behaves similar to that in the homogeneous medium case but plume fall is greatly slowed.

5. CONCLUSIONS

The results of this investigation have illustrated that at realistic groundwater velocities density differences as low as 0.0008 g/cm^3 (1000 mg/L) can cause convective dispersion and instability development under the experimental conditions described herein. As the density difference between DAPLs and ambient groundwater is increased to 0.0015 (2000 mg/L NaCl), 0.0037 (5000 mg/L NaCl), or higher, convective dispersion significantly alters the dispersion process, resulting in a large degree of vertical spreading of the plume. In addition, this transient plume spreading occurs for long times, making it possible for the entire plume to experience changing shapes with time. The three dimensionality of gravitational instability propagation can give rise to high and low concentration zones within the plumes, with the highest concentration zones occurring in the lower portions of the plume.

Heterogeneities at the scale and distribution studied, are seen to retard plume fall. Scale and hydraulic conductivity magnitude and distribution are important as the presence of a high conductivity pathway could accelerate plume fall depending on its size and position. In the case of layered media, small variations

in hydraulic conductivity, on the order of half an order of magnitude or less, can retard gravitational free convection of the DAPL, as mass can build up along horizontal bedding interfaces, resulting in a much less dispersed plume. The gravitational redistribution of mass in a wedge shaped plume front in more dense plumes [density difference of 0.0071 g/cm^3 (10,000 mg/L) and 0.0176 g/cm^3 (25,000 mg/L)] along a bedding interface can result in plume migration velocities up to 34% greater than ambient groundwater velocities for horizontal strata, with greater velocities for dipping strata.

The experiments in the lenticular medium, actually the most realistic example of a relatively homogeneous aquifer, show that while the lenses retard plume fall and mask instability development they also work together with convective dispersion to split up the plume, resulting in a highly dispersed plume. These results also show the scale at which heterogeneities influence flow and the strong influence of small variations in hydraulic conductivity. Plume bifurcations indicate that the detection of shallow plumes does not negate the existence of lower plumes and that plumes may be missed if one samples at a depth that happens to coincide with a "hole" in the plume.

The difficulty of numerically modelling the effect of density variations on plume migration can be seen with the irreproducibility of the size and position of instability propagation or density convection and the effects of small variations in hydraulic conductivity in the physical model experiments. The presence of density differences can therefore entirely change the dispersion process in miscible displacements in saturated porous media and the applicability of Fickian-type laws is thus drawn into question. Although a truly homogeneous medium rarely exists, use of equation (4.1) can give us a means to determine when density effects need to be considered. Finally, the value of physical modelling studies can be seen, provided that they are carried out at realistic groundwater velocities and conditions.

REFERENCES

Bachmat, Y. and D.E. Elrick, Hydrodynamic instability of miscible fluids in a vertical porous column, Water Resour. Res., 6 156-171, 1970.

Bear, J., Dynamics of Fluids in Porous Media, Amer. Elsevier, 1972

Bowles, J.E., Engineering Properties of Soils and their Measurement, pp. 97-104, McGraw-Hill, 1978.

Cahill, J.M., Hydraulic sand-model studies of miscible-fluid flow, J. Res. U.S. Geol. Surv., 243-250, 1973.

Coskuner, G. and R.G. Bentsen, Prediction of instability for miscible displacements in a Hele-Shaw cell, Revue de L'Institute Francais du Petrole, 42(2), 151-162, 1987.

CRC, Handbook of Chemistry and Physics, 62nd ed., CRC Press, Inc., Cleveland, Ohio, 1981.

Das, B., Soil Mechanics Laboratory Manual, pp. 47-52, Engineering Press, 1982.

Davies, P.B., Modelling areal, variable density, ground water flow using equivalent freshwater head - analysis of potentially significant errors, in Proc. Solving Ground Water Problems with Models, Denver, Colorado, pp. 888-903, NWWA, 1987.

de Marsily, G., Quantitative Hydrogeology, 440 pp., Academic Press, 1986.

De Smedt, F. and P.J. Wierenga, Solute transfer through columns of glass beads, Water Resour. Res., 20(2), 225-232, 1984.

Dudgeon, C.R., Wall effects in permeameters, Proc. ASCE, Hydraulics Div., 93 (HY 5), 137-148, 1967.

Freeze, R.A. and J.A. Cherry, Groundwater, 604 pp., Prentice-Hall, 1979.

Herbert, A.W., C.P. Jackson and D.A. Lever, Coupled groundwater flow and solute transport with fluid density strongly dependent upon concentration, Rep. HL87/1347, Theoretical Physics Division, Harwell Laboratory, Oxfordshire, England, 1987.

James, R.V. and J. Rubin, Accounting for apparatus-induced dispersion in analyses of miscible displacement experiments, Water Resour.Res., 8, 717-721, 1972.

List, E.J., The stability and mixing of a density-stratified horizontal flow in a saturated porous medium, Rep. KH-R-11, Calif. Inst. of Technol., Pasadena, 1965.

MacFarlane, D.S., J.A. Cherry, R.W. Gillham and E.A. Sudicky, Migration of contaminants in groundwater at a landfill: a case study, 1. Groundwater flow and plume delineation, J. Hydrol., 63, 1-31, 1983.

Marle, C.M., Multiphase Flow in [illegible]ous Media, 257 pp., Gulf Publishing Company, 1981.

Paschke, N.W., Mean behaviour of buoyant contaminant plumes in groundwater, M.Sc. thesis, 90 pp., University of Wisconsin-Madison, Dept. of Civil and Environ. Eng., 1982.

Paschke, N.W., and J.A. Hoopes, Buoyant contaminant plumes in groundwater, Water Resour. Res., 20, 1183-1192, 1984.

Polivanova, A.I., Contamination of subsurface waters with highly mineralized industrial wastes in the light of experimental data, in Proc. of the Moscow Symposium, August 1971: Actes du Colloque de Moscou, Aout 1971, IAHS-AISh Publ. No. 103, 1975.

Robinson, R.A., and R.H. Stokes, Electrolyte Solutions, Butterworth, London, 1970.

Schiegg, H.O. and J.F. McBride, Laboratory setup to study two-dimensional multiphase flow in porous media, in Proc. Petroleum Hydrocarbons and Organic Chemicals in Ground Water, Houston, Texas, pp. 371-395, NWWA, 1987.

Smart, P.L. and I.M.S. Laidlaw, An evaluation of some fluorescent dyes for water tracing, Water Resour. Res., 13, 15-33, 1977.

Stanbro, W.D. and D.A. Pyrch, Stability of Rhodamine WT in saline water, Water Resour. Res., 15, 1631-1632, 1979.

Sudicky, E.A., R.W. Gillham and E.O. Frind, Experimental investigation of solute transport in stratified porous media 1. the non-reactive case, Water Resour. Res., 21(7), 1035-1041, 1985.

Sudicky, E.A., A natural gradient experiment on solute transport in a sand aquifer: spatial variability of hydraulic conductivity and its role in the dispersion process, Water Resour. Res., 22(13), 2069-2082, 1986.

Todd, D.K., Groundwater Hydrology, 2nd Edition, John Wiley and Sons, New York, 1980.

Wooding, R.A., The stability of a viscous liquid in a vertical tube containing porous material, Proc. Roy. Soc. A, 252, 120-134, 1959.

Wooding, R.A., Free convection of fluid in a vertical tube filled with porous material, J. Fluid Mech., 13, 129-144, 1962.

Wooding, R.A., Convection in a saturated porous medium at large Raleigh number or Peclet number, J. Fluid Mech., 15, 527-544, 1963.

Wooding, R.A., Growth of fingers at an unstable diffusing interface in a porous medium or Hele-Shaw cell, J. Fluid Mech., 39, 477-495, 1969.

APPENDIX

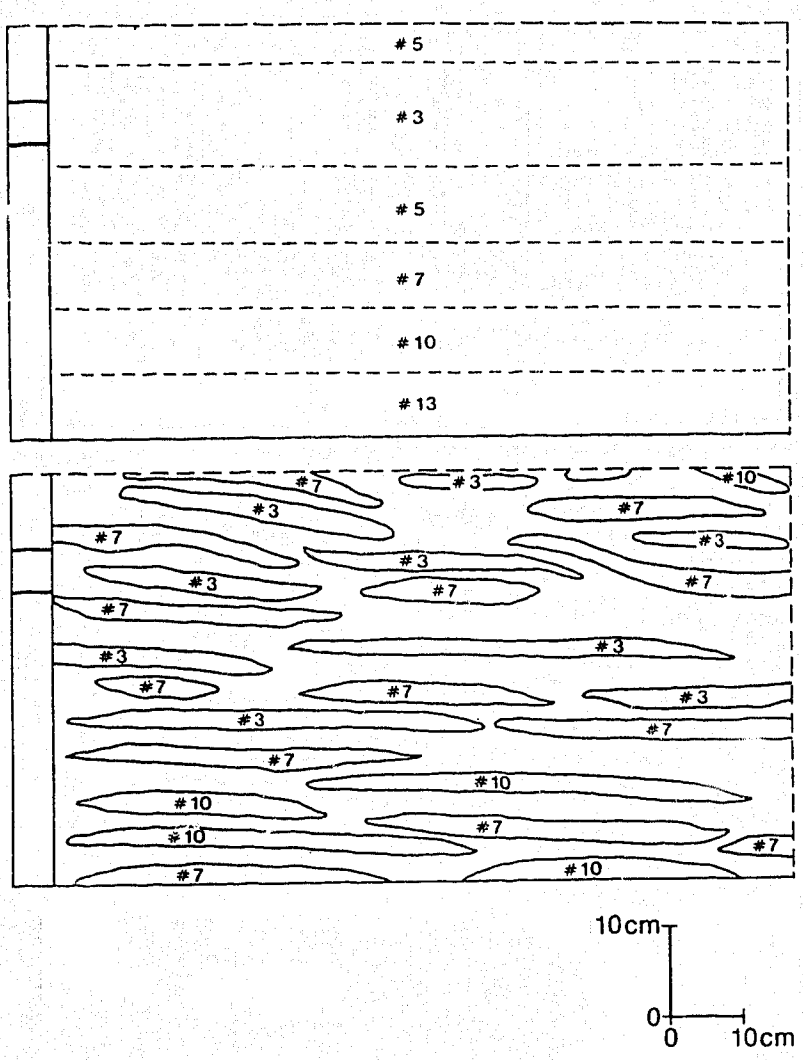

Figure A1. Positions of the Layers and Lenses in an Image Processed Plume.